

Deformation structures associated with the Trachyte Mesa intrusion, Henry Mountains, Utah: Implications for sill and laccolith emplacement mechanisms



Penelope I.R. Wilson ^{a,*}, Ken J.W. McCaffrey ^b, Robert W. Wilson ^c, Ian Jarvis ^a, Robert E. Holdsworth ^b

^a Department of Geography and Geology, Kingston University London, Kingston upon Thames KT1 2EE, UK

^b Department of Earth Sciences, Durham University, Durham DH1 3LE, UK

^c BP Exploration, Chertsey Road, Sunbury-on-Thames TW16 7LN, UK

ARTICLE INFO

Article history:

Received 25 October 2015

Received in revised form

30 March 2016

Accepted 5 April 2016

Available online 7 April 2016

Keywords:

Deformation bands

Faults

Intrusion

Sill

Laccolith

Emplacement mechanism

ABSTRACT

Deformation structures in the wall rocks of igneous intrusions emplaced at shallow crustal depths preserve an important record of how space was created for magma in the host rocks. Trachyte Mesa, a small Oligocene age intrusion in the Henry Mountains, Utah, is composed of a series of stacked tabular, sheet-like intrusions emplaced at 3–3.5 km depth into sandstone-dominated sedimentary sequences of late Palaeozoic–Mesozoic age. New structural analysis of the spatial distribution, geometry, kinematics and relative timings of deformation structures in the host rocks of the intrusion has enabled the recognition of distinct pre-, syn-, and late-stage-emplacement deformation phases. Our observations suggest a two-stage growth mechanism for individual sheets where radial growth of a thin sheet was followed by vertical inflation. Dip-slip faults formed during vertical inflation; they are restricted to the tips of individual sheets due to strain localisation, with magma preferentially exploiting these faults, initiating sill (sheet) climbing. The order in which sheets are stacked impacts on the intrusion geometry and associated deformation of wall rocks. Our results offer new insights into the incremental intrusion geometries of shallow-level magmatic bodies and the potential impact of their emplacement on surrounding host rocks.

© 2016 The Authors. Published by Elsevier Ltd. This is an open access article under the CC BY license (<http://creativecommons.org/licenses/by/4.0/>).

1. Introduction

Shallow-level (<5 km depth) sill and laccolith complexes typically consist of a series of sub-horizontal tabular sheet-like intrusions and form an integral part of sub-volcanic plumbing systems (Cruden and McCaffrey, 2001). Understanding the formation of these networks of sub-horizontal intrusions is, therefore, key to assessing volcanic and sub-volcanic processes such as magma supply and storage in the upper crust (Bachmann and Bergantz, 2008). To-date, significant insights into sill and laccolith emplacement have been made through the characterisation of their geometry and internal architecture using field- and seismic-based data (Du Toit, 1920; de Saint Blanquat and Tikoff, 1997; Thomson, 2004; Thomson and Hutton, 2004; Horsman et al., 2005;

Stevenson et al., 2007a,b; Thomson and Schofield, 2008; Magee et al., 2012). A number of studies have examined the important role played by active faults and shear zones and pre-existing host rock structures in controlling the emplacement and growth of mid-crustal granitic intrusions (e.g. Hutton et al., 1990; McCaffrey, 1992; Neves et al., 1996; Holdsworth et al., 1999; Passchier et al., 2005). Several studies have examined emplacement-related deformation structures associated with the intrusions of the Henry Mountains (Johnson and Pollard, 1973; Pollard et al., 1975; Morgan et al., 2008), but a complete analysis of the geometry, kinematics and sequential development of the wall rock structures has not yet been published.

The Henry Mountains, located in SE Utah on the Colorado Plateau (Fig. 1a), are a type locality for the study of shallow-level igneous intrusions and their emplacement. It was here that Gilbert (1877) famously first described and named laccoliths (coining the term “laccolite”; Gilbert, 1896). Since then, a number of studies have examined the geometries, geochronology and emplacement of intrusions in the Henry Mountains (e.g., Hunt,

* Corresponding author.

E-mail address: penelope.small@gmail.com (P.I.R. Wilson).

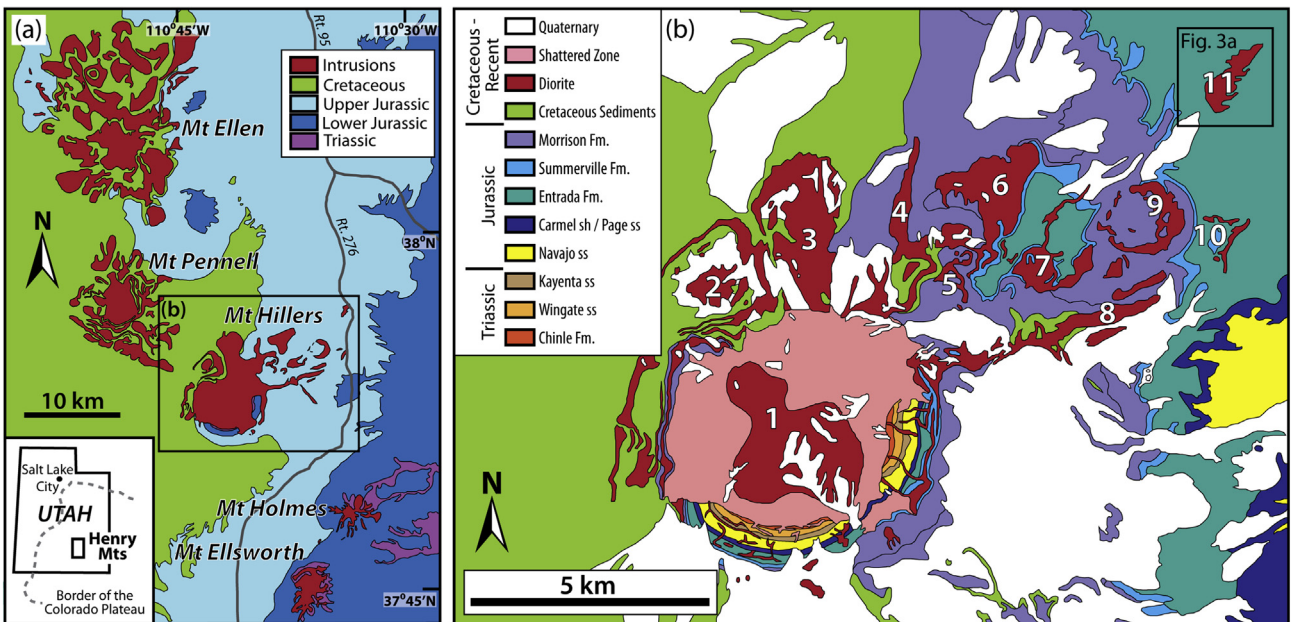


Fig. 1. Simplified regional geological maps of the Henry Mountains. (a) The Henry Mountains region (adapted from Morgan et al., 2008) and its location within Utah (inset map). (b) Mount Hillers and its satellite intrusions (modified from Larson et al., 1985). In (b), the various intrusions that comprise the Mt Hillers intrusive complex are numbered, using the names given by Hunt (1953): 1 – Mt Hillers central complex; 2 – Bulldog Peak intrusion; 3 – Stewart Ridge intrusion; 4 – Specks Ridge intrusion; 5 – Chaparral Hills Laccolith; 6 – Specks Canyon; 7 – speculated feeder system to the Trachyte Mesa intrusion; 8 – Sawtooth Ridge intrusion; 9 – Black Mesa intrusion; 10 – Maiden Creek intrusion; 11 – Trachyte Mesa intrusion.

1953; Johnson and Pollard, 1973; Jackson and Pollard, 1988; Nelson and Davidson, 1993; Habert and de Saint Blanquat, 2004; Horsman et al., 2005; Morgan et al., 2005; de Saint Blanquat et al., 2006; Wetmore et al., 2009; Wilson and McCaffrey, 2013).

Following numerous field studies of the Henry Mountains, Hunt (1953) proposed three general emplacement models for shallow-level intrusions (Fig. 2a–c):

- (1) Radial growth only, with magma emplaced at a constant thickness, and country rocks displaced both vertically and laterally (i.e. Model I, a “bulldozing” mechanism; Fig. 2a);
- (2) Simultaneous vertical and horizontal growth (Model II, Fig. 2b);
- (3) Radial growth of a thin sill, followed by dominantly vertical growth and associated vertical uplift of the overlying host rocks (i.e. Model III, a “two-stage growth” mechanism; Fig. 2c).

Increasingly, evidence suggests that shallow-level crustal intrusions are emplaced and grow through the incremental addition of small volumes of magma, with the amalgamation and stacking of sill-like sheets (e.g. Pitcher, 1970; Mahan et al., 2003; Glazner et al., 2004; Menand, 2008; Morgan et al., 2008). Therefore, the two-stage growth model (Hunt, 1953, Model III) appears most applicable for many larger shallow-level intrusions (i.e. vertical inflation with stacking of sill sheets through under- and over-accretion; Annen et al., 2008; Menand, 2008; Menand et al., 2011). However, for the emplacement of individual sills, all three of Hunt's models (1953) may still be viable.

Corry (1988) highlighted that deformation structures associated with emplacement are potentially strongly linked to the mechanism of emplacement (Fig. 2d–f). A number of studies of emplacement-related host rock deformation have focused on intrusions of the Henry Mountains; these include Johnson and Pollard (1973), Jackson and Pollard (1988), and Morgan et al.

(2008). However, little consideration has been given to the kinematic pathways and associated strains in the wall rocks that can potentially preserve information concerning emplacement mechanisms of individual sills and magma movement (i.e. flow directions).

In this paper, we present a new structural analysis of the geometry, spatial distribution, kinematics, and relative time sequences of host-rock deformation structures surrounding the Trachyte Mesa intrusion, a small satellite intrusion adjacent to the Mount Hillers intrusive complex, Henry Mountains, Utah, USA (Fig. 1b, intrusion 11). By integrating observations of the host-rock structures with the sequential intrusion history, we have created an improved model for the emplacement of Trachyte Mesa that builds on the pioneering studies of Gilbert (1877), and the more recent work of Johnson and Pollard (1973), Morgan et al. (2008) and Wetmore et al. (2009). The results offer new insights into the incremental evolution of intrusion geometries in shallow-level magmatic bodies and how their emplacement leads to deformation of the surrounding sedimentary host rocks.

2. Geological setting

2.1. Henry Mountains

The Henry Mountains Complex consists of five intrusive centres that form the principal mountain peaks in the area. From north to south these are: Mt Ellen; Mt Pennell; Mt Hillers; Mt Holmes; and Mt Ellsworth (Fig. 1a). Most of the intrusions have an intermediate (dioritic) composition (58–63% SiO₂; Hunt, 1953; Engel, 1959; Nelson et al., 1992) and a porphyritic texture, with dominant feldspar (An20–An60; 20–40%) and hornblende (5–15%) phenocrysts. The intrusions are Oligocene in age (31.2–23.3 Ma K–Ar ages; Nelson et al., 1992), and were emplaced into a 3–6 km thick section of late Palaeozoic–Mesozoic predominantly aeolian to shallow-marine sandstones, siltstones and mudstones that overlie

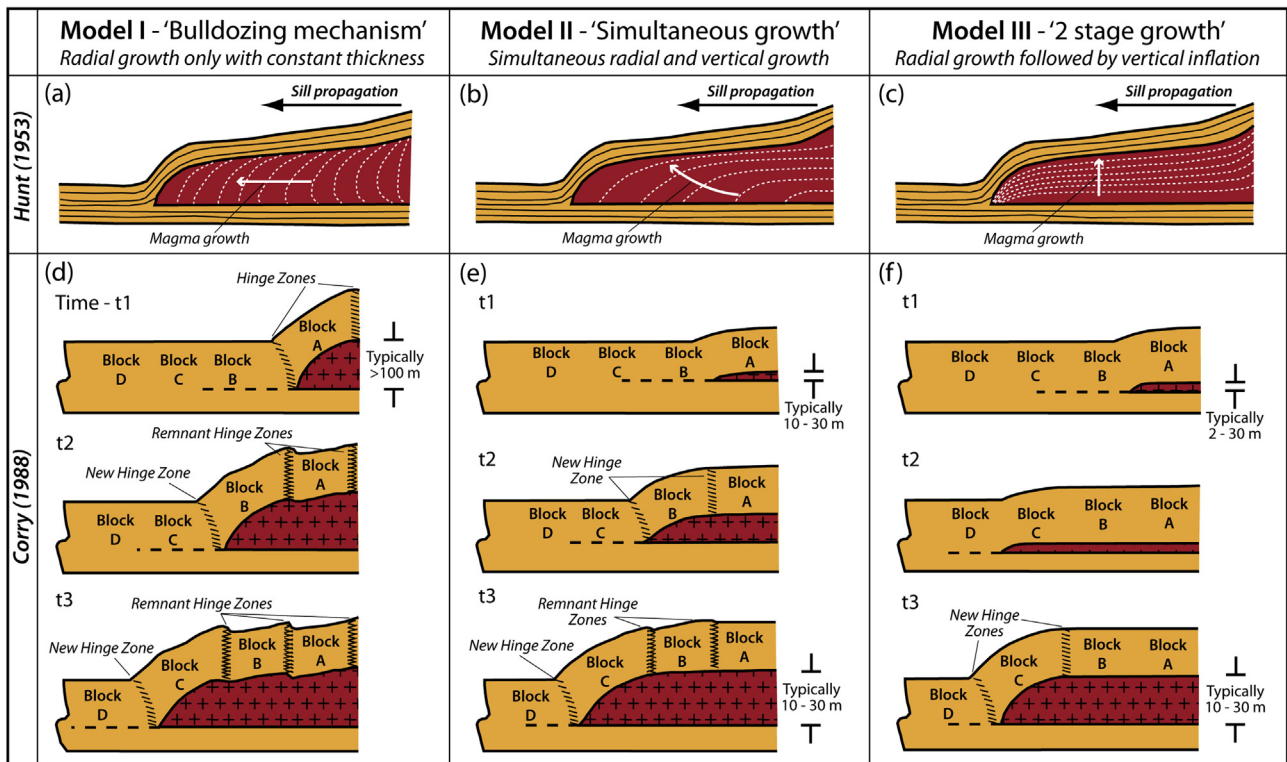


Fig. 2. Growth models for laccolith intrusions (modified from Hunt, 1953, and Corry, 1988). (a), (b) and (c) correspond to Models B, C and A of Hunt (1953) respectively, and show three different mechanisms of laccolith growth: (a) bulldozing; (b) simultaneous growth; and (c) 'two-stage' growth. Based on the three models of Hunt (1953), (d), (e) and (f) correspond to Models 1, 2, and 3 of Corry (1988) for laccolith growth and expected deformation of the country rock.

Precambrian crystalline basement (Jackson and Pollard, 1988; Hintze and Kowallis, 2009). Although Laramide structures (Davis, 1978; Bump and Davis, 2003) occur nearby, the strata into which the Henry Mountains intrusions were emplaced are relatively flat lying (Jackson and Pollard, 1988). The intrusions post-date the locally intense, but more generally weak Late Cretaceous to Paleogene Laramide orogenic activity on the Colorado Plateau (Davis, 1978, 1999). The lack of significant regional tectonism aids the identification of emplacement-related deformation structures and means that the original magmatic and solid-state fabrics are preserved without modification within the intrusive bodies.

2.2. Trachyte Mesa intrusion

The Trachyte Mesa intrusion, referred to as the "Howell laccolith" by Gilbert (Hunt, 1988), is the most distal satellite intrusion of the Mount Hillers intrusive complex, located 12 km to the NE of the central complex (Fig. 1b). The intrusion has an elongate (~2.2 km long and 0.7 km wide) laccolithic geometry, trending c. NE–SW (Fig. 3). Thicknesses observed in cliff exposures range from 5 to 50 m (Morgan et al., 2008), with an average thickness, estimated from magnetic and resistivity studies, of ~15 m (Wetmore et al., 2009). The intrusion is generally concordant with the Jurassic (Callovian) Entrada Sandstone Formation within which it is emplaced (Johnson and Pollard, 1973; Morgan et al., 2008; Wetmore et al., 2009). Emplacement depths for the intrusion are not accurately constrained, although thickness estimates of Hintze and Kowallis (2009) in the area of the Henry Mountains suggest 3–3.5 km of overburden may have been likely. The Entrada Sandstone Formation comprises a mixture of white cross-bedded sandstones, reddish-brown silty sandstones, siltstones, and shales (Aydin, 1978).

Various models have been proposed for the geometry and internal architecture of the intrusion, ranging from a single domal "laccolitic" body (Gilbert, 1877; Hunt, 1953; Wetmore et al., 2009), to a series of stacked intrusive sheets and lobes (Figs. 4 and 5; Johnson and Pollard, 1973; Morgan et al., 2005, 2008).

Detailed mapping of the well-exposed multiple intrusion–host-rock contacts on the top and NW margins of the intrusion suggest that the near-surface form of the magma body strongly influences the present day geomorphology (Morgan et al., 2008). The mesa has a relatively flat top with steeper NW and SE lateral margins. Where exposed, the base of the overall intrusion appears to be relatively concordant with the underlying sandstones, dipping <10° to the NW. Wetmore et al. (2009) suggested that the elongate geometry and trend of the intrusion was controlled by a series of NE–SW trending pre-existing folds, with the central axis of the intrusion located within a synform. NE–SW structures and fabrics are also a key basement trend across the region (Marshak and Paulsen, 1996). Pre-existing structures may, therefore, have played an important role in the trend and geometry of a number of satellite intrusions to the Mt Hillers complex (Fig. 1b; Wilson, 2015), and based on the hypothesis of Wetmore et al. (2009), this may have been important in constraining the planform of the Trachyte Mesa intrusion.

In contrast to the sub-horizontal stratigraphy below the intrusion, the host-rock units above show significant distortion and deformation (Johnson and Pollard, 1973; Morgan et al., 2008). At the NW margin of the intrusion monoclinal bending of the overlying beds is apparent (Figs. 4 and 5a) and has previously been interpreted to be the result of intrusion emplacement (Gilbert, 1877; Hunt, 1953; Johnson and Pollard, 1973; Morgan et al., 2008).

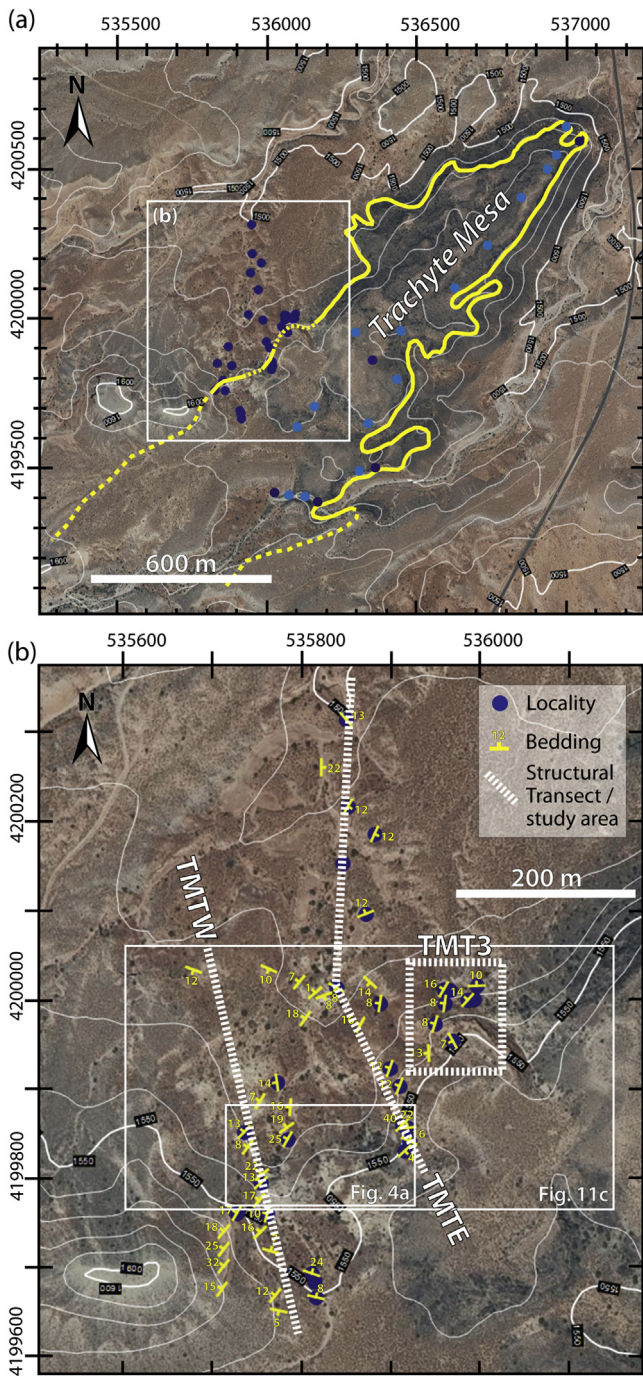


Fig. 3. Maps of the Trachyte Mesa intrusion study area. (a) Contoured and georeferenced aerial image of the Trachyte Mesa area showing the intrusion outline (modified from Morgan et al., 2008). Dashed lines in the SW depict the subsurface extent of the intrusion defined using magnetic resistivity data (after Wetmore et al., 2009). Locations of structural stations are shown by the dark blue filled circles; additional sample stations are shown in light blue. (b) Contoured (heights in metres) and georeferenced aerial photograph (source: <http://gis.utah.gov/data/aerial-photography/>) of field study area, located on the southern end of the NW margin of the intrusion. Structural station localities, bedding measurements, structural transect lines (TMTE, TMTW), and detailed study area (TMT3) are shown. Also see the .kmz file in the Supplementary information for locations of structural stations mentioned within the paper. (For interpretation of the references to colour in this figure legend, the reader is referred to the web version of this article.)

3. Field observations

The present study focused on the southern end of the NW lateral intrusion margin (outlined in Fig. 3) as this area offers the best exposure of the intrusion contacts with the host rocks (Figs. 4 and 5a). Wider reconnaissance (Fig. 3a) of the intrusion found a lack of significant continuous host rock outcrop over the remainder of the intrusion margins. Furthermore, host rocks exposed on the top surface of the intrusion display a distinct lack of deformation structures (Wilson, 2015).

Detailed observations, sampling and structural measurements were carried out on numerous outcrops regularly spaced along two structural transects across the NW margin (Fig. 3b; for individual field localities see .kmz file in Supplementary information). These traverses are referred to here as Trachyte Mesa Transect East (TMTE) and West (TMTW); further observations were made at additional outcrops close to intrusion contacts (including area TMT3; Fig. 3b). At each structural station, a representative structural dataset (deformation type; geometry; kinematics; relative age relationships) was collected with a minimum of 30 measurements per station and >50 in areas of higher intensity deformation.

3.1. Intrusion geometry

Fig. 4 provides an overview of the intrusion contact relationships on the NW margin where structural transects were performed (TMTE and TMTW; Fig. 3b; also see cross-sections in Supplementary information). Multiple stacked sill sheets and sheet terminations may be observed here (Figs. 4 and 5a; see also Morgan et al., 2008). A minimum of 7 and 4 sheets can be observed along TMTE and TMTW respectively (Fig. 4a). It is not possible to map individual sill sheets laterally between the margins along TMTE and TMTW (Fig. 4). Along the eastern transect (TMTE; Fig. 3b) from the NW to SE, the upper sill sheets and the overriding sandstone beds display a distinct monocline geometry with maximum dips of ~40° NW (Figs. 4b and 5a). Lower sub-horizontal sill sheets are also apparent (Fig. 4b). Sandwiched between these upper and lower sill sheets is a zone of highly deformed sandstone with few depositional characteristics preserved. Some sill sheets exhibit “bulbous” terminations (Fig. 4b, c), whilst others display more planar, sub-vertical sheet terminations (Fig. 4d).

The marginal monocline is not developed continuously on the NW intrusion edge. Along the western transect (TMTW; Fig. 3b), ~200 m SW of where the monocline is well exposed, multiple subhorizontal sills can be seen to be stacked one on top of the other (Fig. 4a, d), with terminations stepping back onto the top of the overall intrusive body, forming a “staircase geometry”. Here, the morphology of the bedding in the overlying sandstone appears more complex and step-like, mimicking the sill sheet geometry below (Fig. 4d). An upward-inclined sheet can also be seen here and likely represents an example of sill climbing during emplacement (Fig. 4c). In area TMT3 (Fig. 3b), intrusion contacts are less well exposed, but bedding in the overlying sandstone units has a step-like geometry similar to that seen along transect TMTW.

Terrestrial laser scanning (TLS) techniques (e.g. McCaffrey et al., 2005; Jones et al., 2009; Seers and Hodgetts, 2013) were also used to capture the 3D architecture and spatial distribution of the deformation structures (Fig. 5). High-resolution laser scans were acquired over the intrusion margin in the vicinity of both transects (Fig. 5). The resulting 3D photorealistic models were used to help interpret inaccessible outcrops and to visualise the wider outcrop geometry. See Supplementary information for a fly through movie over the ‘stepped’ western transect (TMTW).

Supplementary video related to this article can be found at <http://dx.doi.org/10.1016/j.jsg.2016.04.001>.

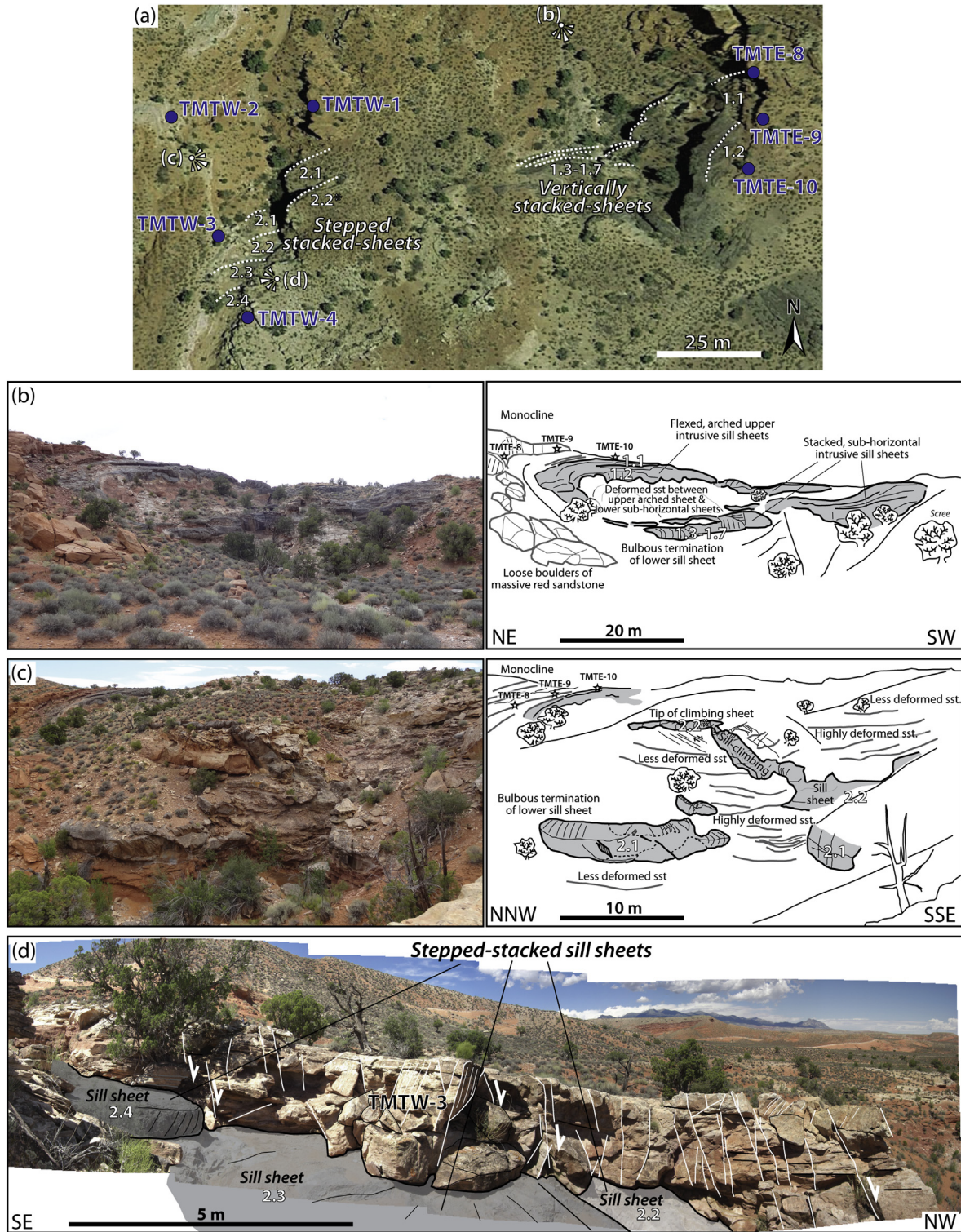


Fig. 4. Photographs and interpretative sketches showing outcrop geometries of stacked sill sheets on the NW margin of Trachyte Mesa. (a) Aerial photograph (Google Earth™) of intrusion margin outcrops. Note contrasting intrusion margin geometries along strike of the intrusion margin (dashed white lines show location of observed sill sheet terminations); vertically stacked-sheets (1.1–1.7) in east of study area (i.e. around TMTE), and stepped stacked sheets (2.1–2.4) in the west (TMTW). Structural stations shown by dark blue filled circles. Note viewpoint locations for photos (b) to (d). (b) View looking SE from structural station TMTE-6 along structural transect TMTE. (c) View looking NE from structural station TMTW-2 onto structural transects TMTW (foreground) and TMTE (in distance). (d) View of structural station TMTW-3, looking NW from viewpoint (d). Key observations to note are: monocline geometry of overriding sandstone units, (b) and (c); flexed/monoclinal upper sill sheets (b) vs. sub-horizontal stacked sill sheets (c, d); sub-horizontal lower sill sheets with “bulbous” terminations (b) and (c); and sill climbing in upper sill sheet, propagating along reverse dip-slip fault (c). (For interpretation of the references to colour in this figure legend, the reader is referred to the web version of this article.)

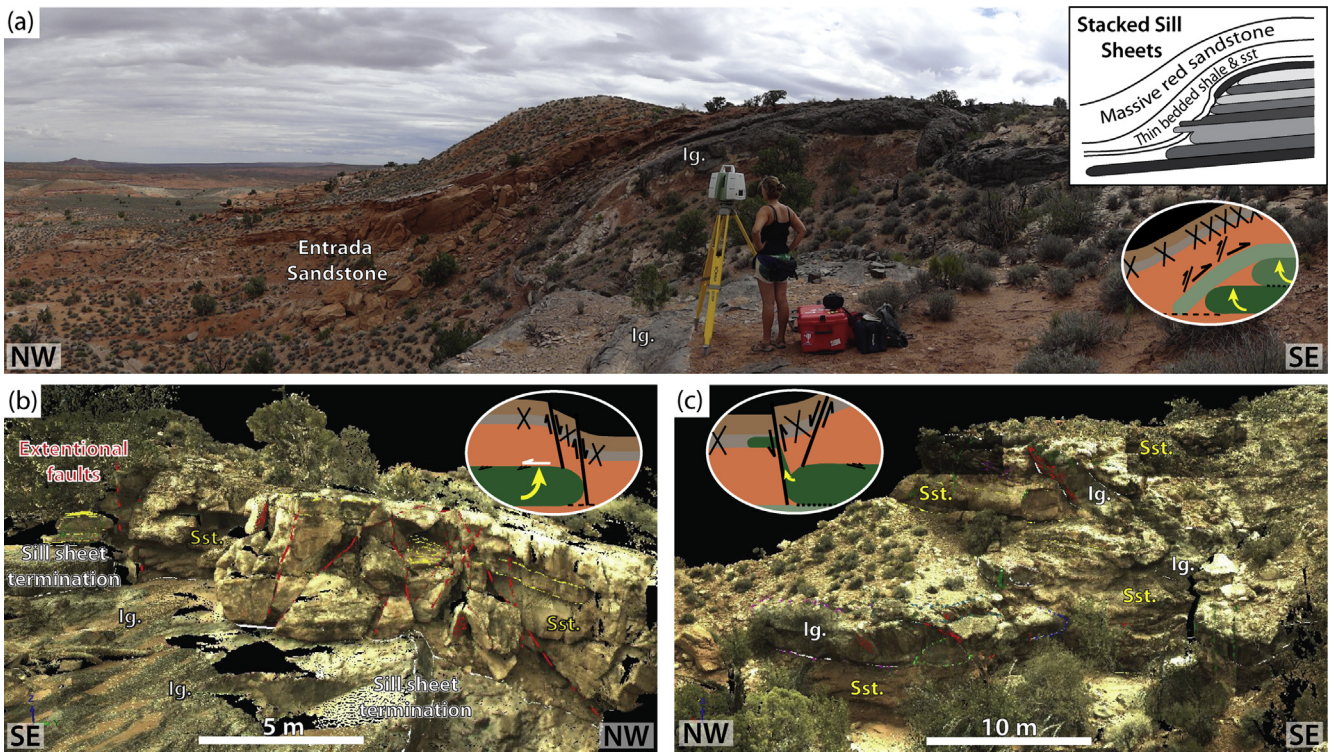


Fig. 5. Terrestrial laser scanning of Trachyte Mesa study area. (a) Field photograph showing monoclonal geometry of the NW intrusion margin along structural transect TMTE (see Fig. 3b for location). Note blocky, red Entrada Sandstone units concordant with the underlying intrusion top surface and stacked intrusive sheets below. Inset (top right), schematic cross section (NW–SE) across the Trachyte Mesa intrusion, showing stacked sill sheets (from Morgan et al., 2008). Inset (bottom right), schematic model of observed intrusion geometries (this study). (b) and (c) Example laser scan interpretations from the Trachyte Mesa intrusion study area showing: (b) a structurally complex zone (structural station TMTW-3; see photo in Fig. 4d for comparison) showing dip-slip faults associated with sill sheet terminations; and (c) a climbing sill sheet, propagating along a syn-emplacement fault (see Fig. 4c for comparison). (For interpretation of the references to colour in this figure legend, the reader is referred to the web version of this article.)

3.2. Deformation structures

3.2.1. Structural types and geometry

Locally deformed bedding forming the monoclinal folds located along the NW lateral margin of the intrusion have dips ranging from sub-horizontal to ~40° NW (Figs. 3b and 6a). Associated small-scale deformation structures in the Entrada Sandstone host rock here include: prolific deformation bands; dip-slip faults; and tensile (Mode 1; Price, 1966) joints (Figs. 6b–d and 7). Most of the deformation bands are porosity-reducing and cataclastic in character (Fig. 8), showing small (mm- to cm-scale) offsets. There is a wide variation in deformation band orientation, with a dominant NE–SW trend, paralleling the margin of the underlying intrusion (Figs. 3a and 6b). Dip-slip faults displaying dm- to m-scale offsets (Figs. 6c and 7d) trend parallel to the local intrusion margins (dominantly NE–SW, and locally ESE–WNW around a small lobe on the NW margin). A more widely distributed system of tensile joints, striking both parallel and perpendicular to the intrusion margin, is also observed (Figs. 6d and 7e, f). These structures commonly show evidence for fluid migration, with fine-grained white carbonate precipitates and/or crystalline calcite spar fills on joint surfaces (Fig. 7g, h).

3.2.2. Structural phases and cross-cutting relationships

Host rock deformation structures observed can be sub-divided into three distinct phases according to deformation structure characteristics and cross-cutting relationships (Figs. 6e–h, 7 and 9).

Phase 1 (P1) structures consist of deformation bands and extensional faults that trend generally oblique (ENE–WSW) to the NE–SW intrusion margin (Figs. 6e and 7a). They are observed over

a wide region, extending well beyond the limits of the underlying intrusions. P1 deformation bands are discrete and are often identified by offsets on bedding and cross-beds. Where significant offsets (cm- to m-scale) are seen, the sense of shear is extensional (Fig. 7a). P1 structures are mostly low- to moderate-intensity structures, with spacings between 50 cm and 100 cm, although high intensity (cm-scale spacing) deformation corridors also occur locally.

Phase 2 (P2) structures are also deformation bands and faults (Figs. 6f–g, 7b–d and 10) that consistently overprint P1 structures (Fig. 9). Both deformation bands and faults trend NE–SW, parallel to the NW lateral margin of the intrusion (Figs. 6f, g and 11). Characteristically, P2 deformation bands commonly form resistant ridges standing proud of the host Entrada Sandstone (Fig. 7c). Microstructural analysis shows them to be largely created as a result of cataclasis and compaction, with significant (almost 100%) porosity reduction (Fig. 8b). The intensity (fracture density) of P2 deformation bands is significantly higher than that of P1, with fracture spacing in the order of 0.5–5 cm, although this decreases rapidly moving away from the intrusion margin. P2 deformation bands typically form conjugate sets with extensional offsets (Fig. 10a, b). Exposed slickenlines on P2 faults suggest dip-slip movements with offsets showing both normal and reverse senses of movement (Fig. 6c, g); NW-side-down offsets are most common (Fig. 10c–e). Unlike P1 extensional faults, distinct principal slip surfaces (PSS; Fig. 10e) and slickenlines are commonly observed (Figs. 6g, 7d and 11). In most cases, P2 deformation bands (Phase 2A) are consistently cross-cut by the dip-slip faults (Phase 2B), as well as by steeply dipping intense deformation corridors (Fig. 10e).

Phase 3 (P3) structures are systems of tensile joints (Figs. 6h and

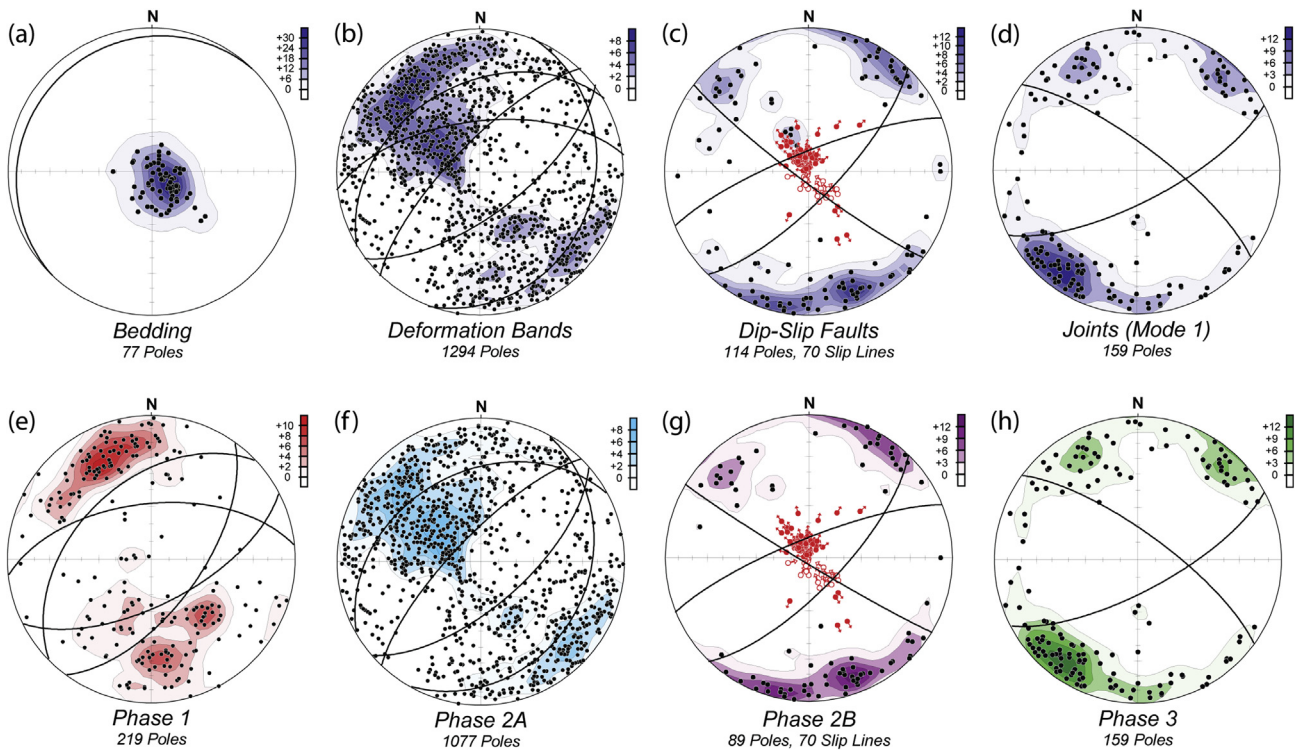


Fig. 6. Summary stereoplots of field structural data. Equal area, lower hemisphere stereoplots of data showing poles to planes (contoured) sorted by structural type: (a) bedding, (b) deformation bands, (c) faults, (d) opening ‘Mode 1’ joints; and structural phase: (e) Phase 1 (P1; deformation bands and faults), (f) Phase 2A (P2A; deformation bands), (g) Phase 2B (P2B; faults), (h) Phase 3 (P3; joints). Mean planes for distinct cluster populations are shown for each plot. Plots (c) and (g) also show fault slip lines with movement direction indicated (red circles with solid fill = normal fault slip; white fill = reverse slip). Contouring intervals are calculated using the ‘Schmidt method’ (Schmidt, 1925; Jowett and Robin, 1988) of grid cell counting (counting circles equal 1% of the area). Contour intervals are percentage values ($n/100)/N = \%$, where n is the number of data points in the cell and N is the total number of data points. (For interpretation of the references to colour in this figure legend, the reader is referred to the web version of this article.)

7e–h), often infilled with sparry calcite, which overprint all other deformation features (Fig. 9c, d). Two sets of joints are recognised trending NW–SE and NE–SW, perpendicular and sub-parallel to the intrusion margin, respectively (Figs. 6 and 7e, f). No systematic cross-cutting relationship is apparent between these two joint sets.

4. Spatial distribution of structures

4.1. Structural transects

The three phases of deformation structure described above have very distinctive distributions relative to the location of the igneous intrusions along the western and eastern transects (TMTW and TMTE; for structural cross sections see [Supplementary information](#)). P1 deformation structures are only clearly recognised at structural stations distal to the intrusion margin. These are progressively overprinted by Phase 2A, 2B and 3 deformation structures with increased proximity to the intrusion. P2 structures increase in intensity from just outboard of the intrusion margin, and onto the top surface of the intrusion.

Bedding along the western transect displays a “staircase geometry” with each step appearing to be associated with a new intrusive sill sheet below (Figs. 4d and 10d). Deformation structures vary across these ‘stepped’ zones: P2A deformation bands are widely distributed across the entire margin; while P2B structures (faults and steep deformation corridors) are localised to the “step” zones at sill sheet terminations (Fig. 10d, e). In contrast, bedding geometry appears simpler along the eastern transect where a clear monoclinal structure can be observed. P2B faults are not observed along this transect. P2A conjugate deformation bands occur along

both transects and rotate about a horizontal axis in the vicinity of stepped-zones and across the flanking monocline (Fig. 10a).

4.2. Variations in deformation structures with intrusion margin trend

P2B faults are observed both along the western transect and also in study area TMT3 (<200 m east of transect TMTE; Fig. 3b). Along the western transect these are associated with the tips/terminations of intrusive sheets (Fig. 10d, e), while in area TMT3 the intrusion does not crop out, but may be inferred using magnetic data collected by Wetmore et al. (2009). Mapping of P2B along strike reveals an arcuate trend that appears to match the proposed curved nature of the ‘lobe’/promontory of the underlying stacked intrusive sheets (Morgan et al., 2008; Wetmore et al., 2009) emanating from the main NE–SW intrusion trend (Fig. 11).

4.3. Deformation structures at the intrusion contact

Distinctive shear zones are observed within and on the top surface of the intrusion, a number of which were described by Morgan et al. (2008). Within the host-rock these are restricted to a reddish-brown silty sandstone and shale unit that is commonly observed immediately above the intrusion, and are not observed in the overlying more massive red sandstones (Fig. 7b). In the upper few centimetres of individual intrusive sheets, and at the interface between the intrusive sheets, a strongly foliated (sub-horizontal foliation) zone occurs with significant stretched plagioclase phenocrysts (Fig. 12).

Thin section analyses of the deformation microstructures within

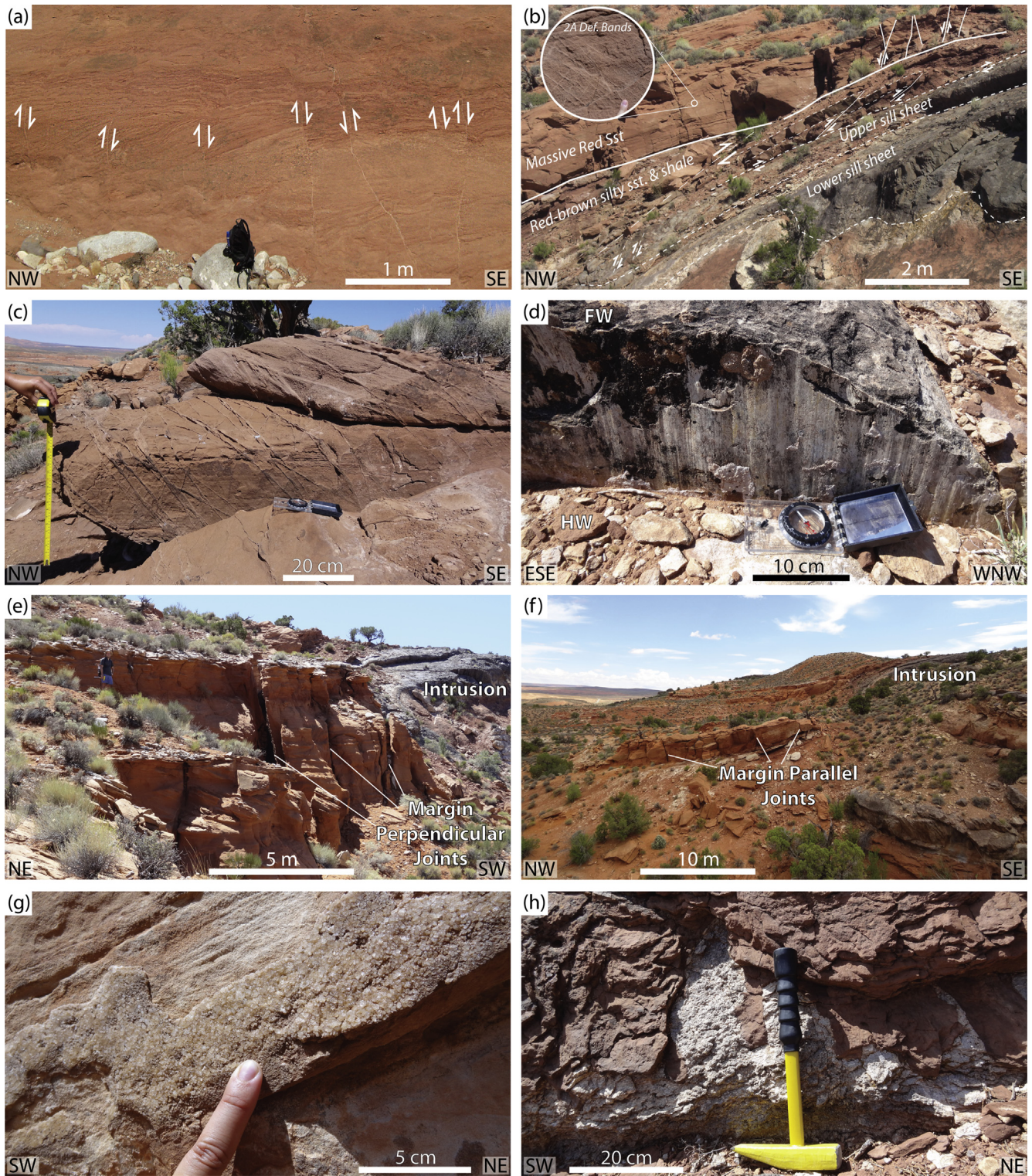


Fig. 7. Annotated field photographs showing examples of Phase 1 (a), Phase 2 (b-d), and Phase 3 (e-h) deformation structures. (a) Background deformation bands cutting the Entrada Sandstone distal (~500 m to the NW; TMTE-0) to the intrusion (0.2–2 m spacing). (b) Deformation structures at intrusion contact, locality TMTE-9 in Fig. 4. Low angle shear and reverse faults (top-to-the-SE) on top surface of the intrusion and within the highly deformed shaly red sandstone layer adjacent to the contact. Extensional conjugate deformation bands in massive red sandstone (also see Fig. 10 in Morgan et al., 2008). (c) Closely spaced porosity reducing deformation bands in massive red sandstone, localised to host rocks overlying the intrusion margin (0.5–5 cm spacing). (d) Dip-slip normal fault (down-to-the-NW) with well-preserved slickenlines on principal slip surface. (e) Opening 'Mode I' joints trending perpendicular to the intrusion margin (NW–SE), 0.5–2 m spacing. (f) Opening 'Mode I' joints trending parallel to the intrusion margin (NE–SW), 1–2 m spacing. (g) Calcite crystals precipitated on margin parallel joint surfaces in (f). (h) 'Flame-like' features comprised of hydrous minerals exploiting sub-vertical joints (P3) on the top surface of the intrusion. (For interpretation of the references to colour in this figure legend, the reader is referred to the web version of this article.)

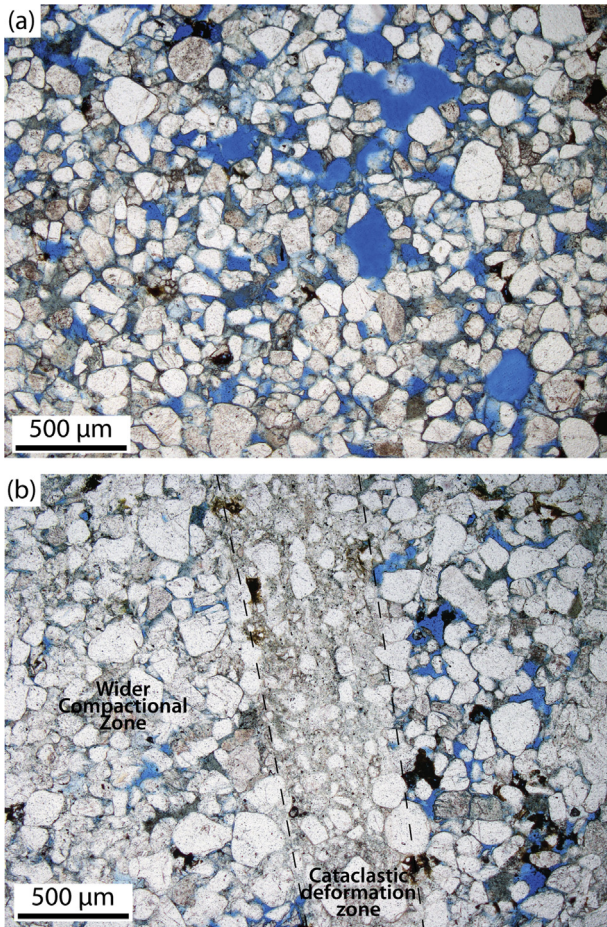


Fig. 8. Photomicrographs of Entrada Sandstone (blue resin infilling pore space). (a) Relatively undeformed parent host rock showing significant pore space; 18–20% porosity. Photograph taken using plane polarized light (ppl). (b) Section across deformation band showing two distinct zones: a narrow (0.5 mm) cataclastic deformation zone characterised by a wide range of grain sizes, angular grains and a fine-grained matrix resulting from grain size reduction; and a wider compactional zone. Porosity reduction is nearly 100% within the cataclastic deformation zone, while within the compactional zone reduction ranges from 75 to 90% (i.e. <5% porosity). Photograph taken under ppl. (For interpretation of the references to colour in this figure legend, the reader is referred to the web version of this article.)

the sheared upper contact of the intrusion show predominantly brittle, and to a lesser extent brittle-ductile, deformation structures (Fig. 12). Where the contact between intrusive sheets and the host rock can be observed, three distinct layers can be defined (Fig. 12; from top to bottom): (1) a 5–10 cm thick baked sandstone layer; (2) a <1 cm thick chilled intrusion margin; and (3) a 1–2 cm zone of aligned (NW–SE) stretched plagioclase phenocrysts, beneath which mineral alignment decreases significantly. Low-angle fracture planes bisect the baked sandstone horizon (Fig. 12a) but do not extend into the intrusion. These fracture planes trend parallel to the intrusion margin (NE–SW), and dip shallowly (~20°) to the SE (Fig. 12a). Slickenlines consistently show SE-side-down kinematics.

These low-angle structures are interpreted to be Riedel shear (R_1) fractures consistent with a top-to-the-SE shear sense. Microstructural analysis of the stretched feldspar phenocrysts developed on the top surface of the intrusive sill sheets (Fig. 12b) reveals brittle shearing of the phenocrysts along multiple fracture planes (Fig. 12c, d). The kinematics of these fracture planes are also consistent with Riedel shear fractures associated with top-to-the-SE (140°) shear (Fig. 12d–f).

Exposed sill terminations fall into two categories: those with more rounded, “bulbous” terminations; and those with steeper, “fault-controlled” terminations. Microstructural analysis of samples collected at the tip and frontal edge of the intrusion contact reveal the presence of sub-vertical fractures and shear bands (with NW-side-down kinematics) consistent with the larger dip-slip faults observed in outcrop (Fig. 13). Stepped intrusion geometries are observed at the micro-scale (Fig. 13c), with steps appearing to be associated with sub-vertical shear-fractures within the host rock (Fig. 13b–e). These fractures can sometimes be seen to extend for a small distance (~500 µm) into the intrusion. Furthermore, magma can also be seen exploiting these sub-vertical shear-fractures (Fig. 13e).

5. Kinematic analysis

Kinematic indicators on P2B dip-slip faults include offsets of bedding plane markers, and steps on slickenlines preserved on fault surfaces (Figs. 6g, 10 and 11). The dip-slip faults record both normal and reverse shear sense, with a predominant NW-side-down movement, consistent with NW–SE extension or flexure across the margin of the intrusion (Fig. 10c–e). Senses of slip on P2A deformation bands mirror the kinematics of the P2B faults (Fig. 10a, b), although they are distributed more widely across the intrusion margin. Conjugate sets of extensional deformation bands commonly have an inclined acute bisector axis, consistent with either an original moderately inclined σ_3 axis dipping towards the NW, or alternatively with rotation of an originally more flat-lying bisector about a broadly horizontal axis post-formation (Fig. 10a, b).

Stress inversion has been carried out following the Minimized Principal Stress Variation method developed by Reches (1987) using MyFault™ software. This method assumes that the stress required to cause fault slip obeys a Coulomb yield criterion. It is reasonable to use such an approach as the overall finite strains recorded here are low, meaning that any rotations of stress axes will be relatively minor (e.g. De Paola et al., 2005). Bulk inversion suggests that the main stress acting on these faults was extensional (i.e. sub-vertical σ_1), with NW–SE (margin perpendicular) oriented extension (Fig. 11). Inclination of the stress axes likely reflects the flexural component of this extension due to rotation of the host rocks during magma emplacement ($\sigma_3 = 338/20$; $\sigma_1 = 160/70$), with extension inclined down towards the NW. Spatial variations are observed in the orientation of dip-slip faults, and the stress inversion of these individual fault populations reveals a change in the local extensional directions along the intrusion margin (extension varying from NW–SE to NNE–SSW; Fig. 11c). These changes in the stress field mimic changes in the orientation of the intrusion margin.

6. Discussion

6.1. Significance and origin of the deformation phases

Since P1 structures do not show any significant spatial or geometric affinity to the Trachyte Mesa intrusion, we suggest that they are likely to have developed prior to emplacement. This is also supported by the consistent cross-cutting relationship observed in the field (i.e. P2 overprinting P1). P1 deformation structures could be attributed to one or more of a number of late Cretaceous to early Tertiary Laramide uplift deformation events observed locally (e.g. see Bump and Davis, 2003).

The strong spatial, geometric and kinematic relationship between the P2 structures and the location and orientation of the intrusion margins suggests that this deformation is related to the emplacement of the Trachyte Mesa intrusion. P2B faults and steep

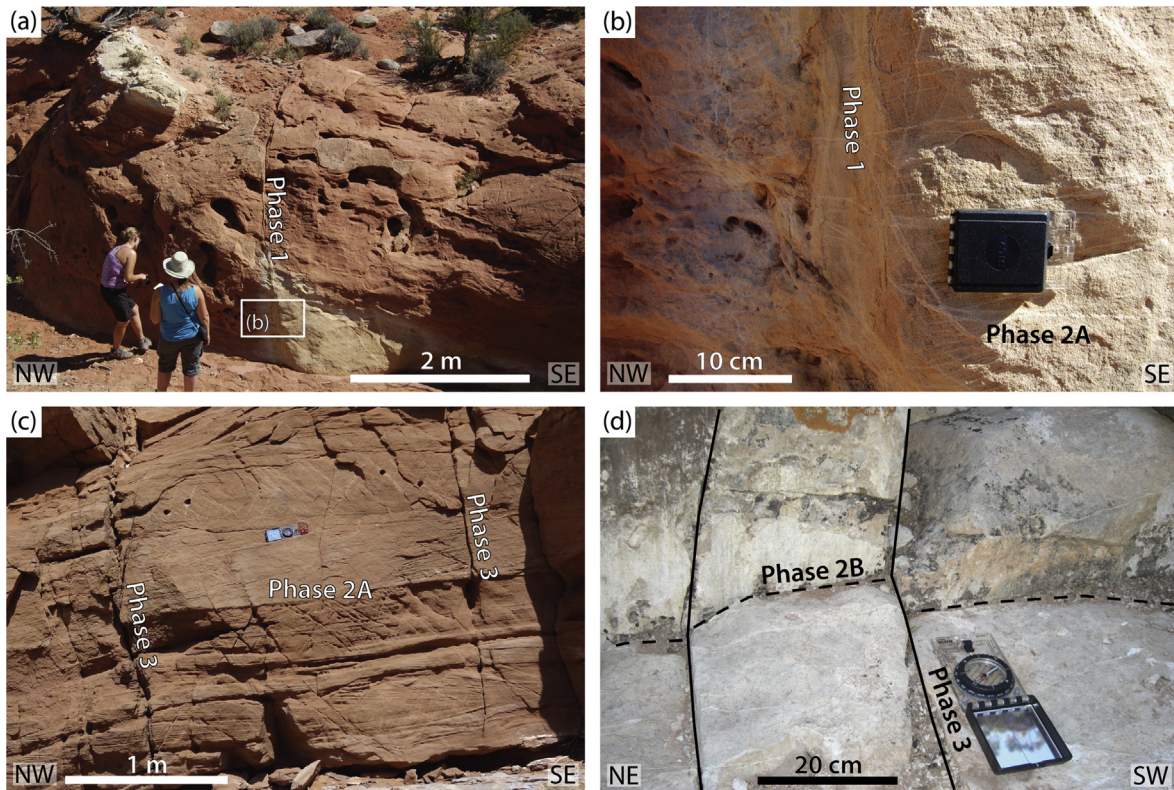


Fig. 9. Cross-cutting relationships between structural phases. (a) Example of large P1 deformation band observed at structural station TMTE-4. (b) Close-up view of deformation band shown in (a), note the second system of deformation bands (P2A) cross-cutting the steeply dipping P1 set. (c) Conjugate deformation bands (P2A) cross-cut by steeply-dipping P3 joints (TMTE-9). (d) Steeply dipping extensional faults (P2B) cross-cut by P3 joints (TMTW-3).

deformation corridors overprint the more widespread P2A deformation bands. As observed along the western transect, P2A deformation bands are distributed across the entire intrusion margin, whereas P2B faults are predominantly localised at sill sheet terminations. We suggest that this is a result of strain localisation within the overburden during vertical inflation of the underlying sill sheet. We therefore interpret that P2B structures are accommodation structures associated with vertical inflation of individual sill sheets. The observed monocline geometry, and the distribution and style of deformation, matches closely to mechanical models of steeply dipping (extensional) forced folds (Withjack et al., 1990; Johnson and Johnson, 2002).

P3 tensile joints overprint all other structures. We propose that the joints are most likely associated with deflation and possibly cooling of the host rocks as the magma body beneath cooled, crystallised and contracted. This origin for the P3 joints fits with their wide spatial distribution over the intrusion, in contrast to the P2B faults, which are entirely localised around sill terminations. A late-stage emplacement timing for the formation of the joints, rather than post-emplacement, is supported by the presence of calcite crystals on joint surfaces (Fig. 7g), and hydrothermal fluid escape structures (Fig. 7h) observed on the top surface of some intrusive sheets, suggesting that these joint sets must have developed while hydrothermal fluids associated with the intrusion were still circulating.

6.2. Faults at sill terminations

A significant observation from this study, previously undocumented at Trachyte Mesa, is the presence of dip-slip faults associated with individual sill terminations (i.e. P2B structures). Thomson

and Schofield (2008) suggested that the main control on the development of faults at sill sheets terminations is the depth of emplacement. At shallower depths, cohesive strength along bedding planes is less, and so favours the development of flexural slip folds. At greater depth, higher shear stresses are required for flexural slip, thus potentially favouring mechanical failure of the rock through fracture/faulting (Stearns, 1978). The overburden thickness estimated for the Trachyte Mesa by Hintze and Kowallis (2009) suggests that the Entrada Sandstone would have been at a paleodepth of ~3 km at the time of magma emplacement, therefore placing it within the brittle zone (as defined by Schofield et al., 2012).

Pollard and Johnson (1973) presented a conceptual model for the formation of peripheral dykes located at the tips of laccolith bodies from field observations. It was suggested that the dykes formed at the periphery of the intrusions as a result of flexural/elastic bending of the overburden layers (contractional over the centre and extensional over the periphery). The observed sill-climbing structures at Trachyte Mesa fit with the development of extensional strains at the intrusion periphery. However, instead of the strain being accommodated by simple opening 'Mode 1' joints, it is proposed here that the mostly extensional P2B faults were exploited by the magma (Figs. 4b and 5c).

6.3. Modes of emplacement

If the magma in a sill sheet intrudes radially at a constant thickness ('bulldozing'), the resulting host rock deformation will be predominantly compressional and should be distributed over the entire extent of the intrusion (i.e. margins and top surface; Fig. 1a; Corry, 1988). A two-stage model, comprising lateral spreading of a

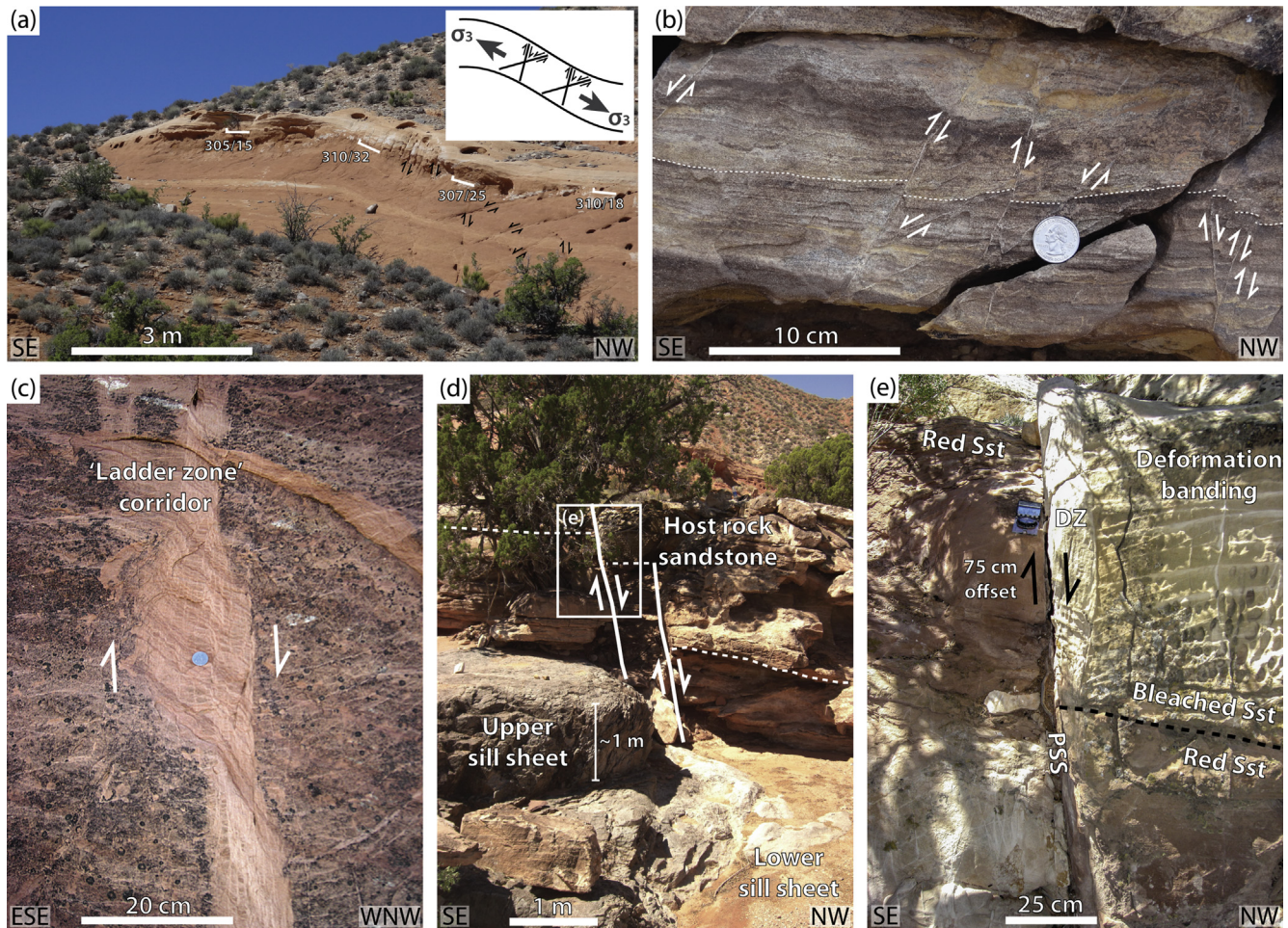


Fig. 10. Annotated field photographs showing additional examples of P2A (a–b) and P2B (c–e) structures and kinematics. (a) Monoclinal bedding geometries in sandstone units ~30 m above the intrusion, showing conjugate fault/deformation band geometries consistent with flexure (note offset on bedding in paler sandstone unit). (b) Outcrop example (~5 m above intrusion) of conjugate deformation banding showing consistent offsets to those seen in (a). (c) Steep deformation corridor/ladder zone (down-to-the-NW shear) overprinting conjugate deformation bands. Note kinematics of background deformation bands and ladder zone are the same. (d) Outcrop example of normal faults developed at the termination of sill sheets. Note total throw on normal faults is roughly consistent with the thickness of the individual sill sheet, implying that the faults may be induced by sill sheet inflation. (e) Close-up of area outlined in (d) showing ~75 cm normal (down-to-the-NW) offset of bedding contact (PSS – Principal Slip Surface; DZ – Damage Zone).

thin sheet followed by vertical inflation, will lead to deformation being localised within the high-strain hinge zones located at the intrusion margins, and to a mixture of compressional and extensional strains (Fig. 1c). This latter model is consistent with the kinematics and spatial distribution of deformation structures described here, suggesting that these features are closely related to the mode of emplacement. Our observations support a stacked sill sheet growth model for the overall intrusion with a two-stage growth model for individual sheets. We prefer this model as there is no evidence for remnant hinge zones on the top surface of the intrusion, which would be expected for both ‘bulldozing’ and simultaneous sill intrusion growth models.

We envisage that individual sill sheets were emplaced close to their full radial extent as thin sheets that then vertically inflated through additional magma influx. The contrasting deformation styles observed likely reflect different deformation processes taking place in the intrusion-contact zone (simple shear dominated strain) and the surrounding host rocks (pure shear extension dominated deformation) during emplacement. Simple shear fabrics and deformation at the intrusion contact are most likely driven by magma flow and associated flattening, whilst the wider extensional deformation accommodates the additional rock volumes required

during sill sheet inflation.

6.4. Emplacement and structural evolution

Based on the work of previous authors (Corry, 1988; Morgan et al., 2008) and our new field observations of intrusion geometries and deformation structures, a new multistage model for the emplacement of the Trachyte Mesa intrusion is proposed (Fig. 14).

6.4.1. Stage 1 – onset of sheet emplacement and radial growth of a thin “proto-sill” sheet

It is proposed that a magma feeder system propagated vertically through the sedimentary pile until it reached a suitable interval for a horizontal sheet to propagate laterally. In the case of Trachyte Mesa, this interval corresponds to a thin, mechanically weak, reddish-brown silty sandstone and shale layer occurring between thicker, massive sandstone units (Fig. 7b; Morgan et al., 2008). The “proto-sill” propagated as a thin sheet (poorly constrained, but assumed to be <25 cm), with minor inflation, to its maximum lateral extent (Figs. 14 and 15a). The extent of lateral propagation of magma is controlled by a number of factors, including host rock fracture toughness, magma supply and flux, and freezing processes

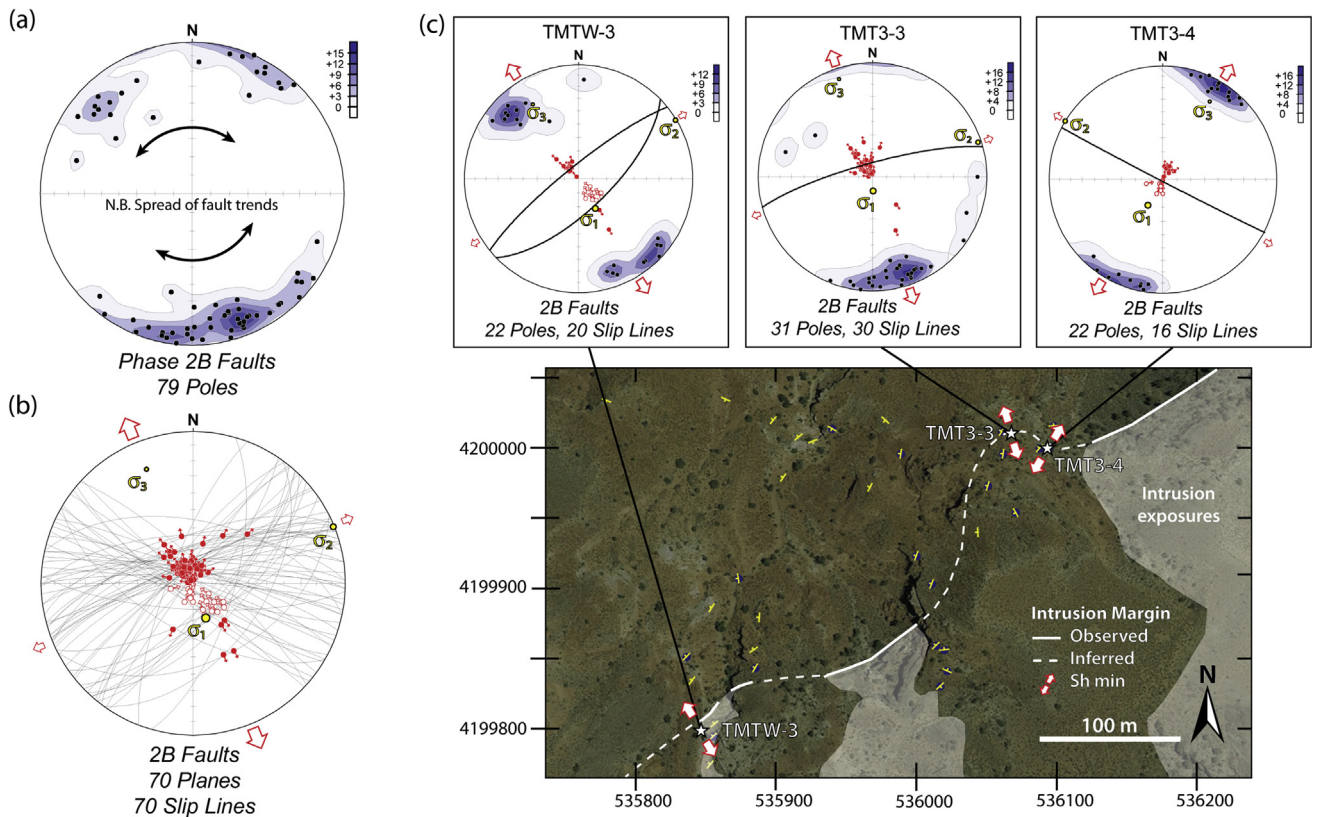


Fig. 11. Structural data and map demonstrating the arcuate trend of Phase 2B faults. (a), (b) Equal area lower hemisphere stereoplots showing all fault trends of P2B faults. Faults show dip-slip normal and reverse movements, consistent with NW–SE extension (note inclination of σ_3 , associated with flexure along the intrusion margin). (c) Map showing the distribution of the main outcrop localities at which P2B fault data were collected. The change in geometry and kinematics of the faults with the changing trend of the intrusion margin can be seen from the equal area lower hemisphere plots for each outcrop showing poles to planes, slickenlines and interpreted kinematics. Solid white lines depict areas where intrusion margin is exposed, dashed white lines show inferred continuation of margin beneath sandstone beds [magnetic data from Wetmore et al. (2009) was used to guide this subsurface geometry]. See Fig. 3b for location in context of wider area.

in the sill tips (Bunger and Cruden, 2011). Bunger and Cruden (2011) showed through mechanical modelling that magma viscosity is not a major influence on sill dimensions. The presence of blunt and bulbous terminations at Trachyte Mesa indicate such freezing processes in the sill tips, and with this an increase in fracture toughness (Johnson and Pollard, 1973; Morgan et al., 2008; Bunger and Cruden, 2011).

Deformation associated with early emplacement is likely to have been minor, and dominated by shear at the proto-sill sheet contacts. As magma flowed in a NE direction, spreading out radially to the NW and SE, shear zones developed on the top and base surfaces of the intrusion and its contacts with the surrounding host rock. These shear structures show both brittle and plastic deformation characteristics due to the effects of hot magma being emplaced into a cold host rock. Vergence on these shear structures is opposite to the flow direction of the magma sheet (i.e. on the NW margin, top-to-the-SE-verging shear fabrics occur on the top surface of the intrusion). These shear fabrics can be seen both at outcrop and in thin section (Fig. 12), and have also been defined by AMS (Anisotropy of Magnetic Susceptibility) studies (Morgan et al., 2008). According to this model, shearing at the intrusion margin is the first-formed accommodation structure related to the onset of sheet emplacement.

6.4.2. Stage 2 – vertical inflation of sill sheet

Once the magma had reached its maximum radial extent, vertical inflation commenced as magma supply continued. The thickness of the sill will be governed by the thickness of the overburden

(i.e. lithostatic pressure) and the magma pressure (Corry, 1988; Thomson and Schofield, 2008).

Pollard and Johnson (1973) showed that for similar Henry Mountains laccoliths (e.g. Buckhorn Ridge and Black Mesa intrusions) the effective overburden thickness was somewhere between 300 and 500 m, significantly less than the true overburden thickness (Figs 6 and 25 in Pollard and Johnson, 1973). This is due to the effect of stratification, the elastic moduli of different formations, and how well these bond together. Taking into consideration all of the above, once the horizontal length is roughly equal to the effective thickness of the overburden, a change to laccolith intrusion mechanisms would be expected with continued magma flux (Cruden and McCaffrey, 2006; Bunger and Cruden, 2011). Therefore vertical displacements would take over from horizontal propagation. Using the planform horizontal extent of the Trachyte Mesa intrusion, and assuming that sill sheets radiate outwards from a central NE–SW trending intrusion axis (Morgan et al., 2008), the intrusion half-width is ~250 m. In order for laccolithic processes to take over, an equivalent ~250 m effective overburden thickness would be required. This corresponds closely to base of the Morrison Formation (Johnson and Pollard, 1973; Hintze and Kowallis, 2009). As this defines a significant change in lithostratigraphy, a corresponding change in elastic moduli would be expected.

Thickening of the sill sheet resulted in roof uplift and deformation (e.g. P2 fractures and deformation bands associated with forced folding and flexural bending) of the overlying strata (cf. Stearns, 1978; Cosgrove and Hiller, 1999; Galland et al., 2009; Magee et al., 2014). Conjugate sets of extensional cataclastic

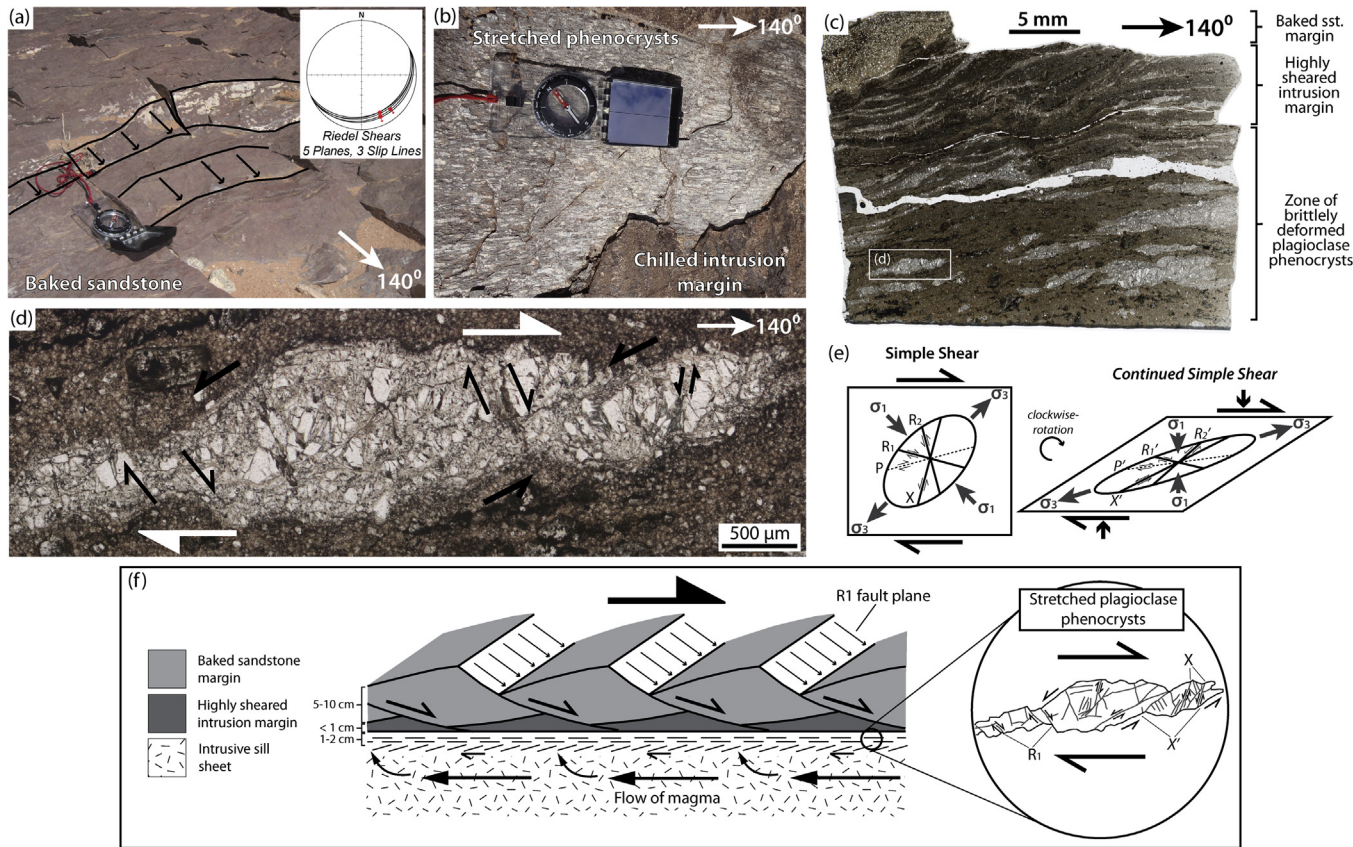


Fig. 12. Flow generated fabrics at the intrusion margin. (a) Outcrop photograph showing low-angle brittle extensional faults (see inset stereoplot) cutting baked sandstone unit on top surface of an intrusive sheet. These are interpreted to be equivalent to R_1 Riedel shear planes, depicted in (d). The faults are only apparent in the baked sandstone and appear to terminate at the intrusion-host rock interface. (b) Stretched plagioclase phenocrysts within a strongly sub-horizontal foliated zone (2–3 cm) on the top surface of an intrusive sheet. Note also the thin (<1 cm) chilled margin zone above the stretched phenocryst/foliated layer. (c) Photograph of thin section (ppl) across sheared intrusion top surface. (d) Photomicrograph (ppl) of deformed, elongate plagioclase phenocryst within the uppermost 2–3 cm of an intrusive sheet (note section is cut along a vertical plane oriented parallel to the stretching direction, 140° – 320°). The phenocryst is deformed mainly by brittle deformation and a series of preferred deformation planes, with offset, can be identified. The movement and orientation of these planes are consistent with Riedel fractures associated with top-to-the-right (SE) sub-horizontal shear. (e) Diagram illustrating incremental strain associated with simple-shear deformation. Image on left shows initial configuration of Riedel shear fractures, while image on right shows orientations after continued simple shear and flattening (20% pure shear). Note clockwise rotation of fractures. (f) Schematic cartoon depicting the deformation structures observed at outcrop and in thin section on the top surface of an intrusive sheet. The structures and kinematics are consistent with top-to-the-SE sub-horizontal shear. This shearing is likely driven by magmatic flow within the underlying sheet, leading to sub-horizontal shortening and shear at the intrusion contact.

deformation band structures (P2A; Figs. 6, 7, 10 and 11) formed in the overlying massive sandstone beds, localised in the region of the developing lateral margin, increasing in intensity around the monoclinal flank above the sill termination (Fig. 14). This is consistent with extensional deformation structures forming in the outer arc areas of monoclinal flexural folds, while contractional structures will be dominant in the inner arc areas (Frehner, 2011). This extension and contraction in the outer and inner arcs, respectively, may help to explain the observation that deformation within the blocky sandstone units is predominantly extensional, while in the more shaly units at the intrusion contact, reverse faults occur (Fig. 7b; also noted by Morgan et al., 2008).

Although lateral propagation of the sill is likely to have ceased during this inflation phase of emplacement, shear structures may still have continued to develop on the top surface of the intrusion due to magma flow. Fig. 12 shows examples of shear structures on the intrusion top surface. As these brittle structures clearly deform already cooled rock, this shear deformation is post-initial emplacement. However, in order to accommodate the additional volume of magma, shear strain on the top surface will have become dominated by flattening (vertical shortening). This is apparent in the stretching and flattening of plagioclase crystals within the

upper 2–5 cm of the sill sheet (Fig. 12c, d).

As vertical inflation continued, strain became localised at the sill sheet terminations resulting in the formation of P2B structures (Figs. 10, 11 and 14). This strain localisation led to the development of steep deformation corridors cross-cutting earlier conjugate deformation bands (Fig. 10c) and, eventually, the development of principal slip surfaces and dip-slip faults (Figs. 10d, e and 15b). These P2B dip-slip faults observed at Trachyte Mesa therefore played a significant role in accommodating the extra volume of magma within the crust.

It is proposed that the smooth, curved nature of the “bulbous” sill sheet terminations (Fig. 4c; Morgan et al., 2008) are the result of inflation (Fig. 15b). This rounded geometry is only observed for sill terminations that formed within clay-rich, shaly red sandstones (weaker), whilst more abrupt, “fault-controlled” vertical terminations are found in closer proximity to the overlying competent red and bleached sandstones (stronger). The differences in lithology and their mechanical properties are therefore likely to have played a significant role in the type of sill sheet termination.

An igneous sill propagating in an elastic/brittle medium, as is the case here, should have a tapered or wedge-shaped tip (Fig. 15a). Both the “bulbous” and “fault-controlled” tip terminations are,

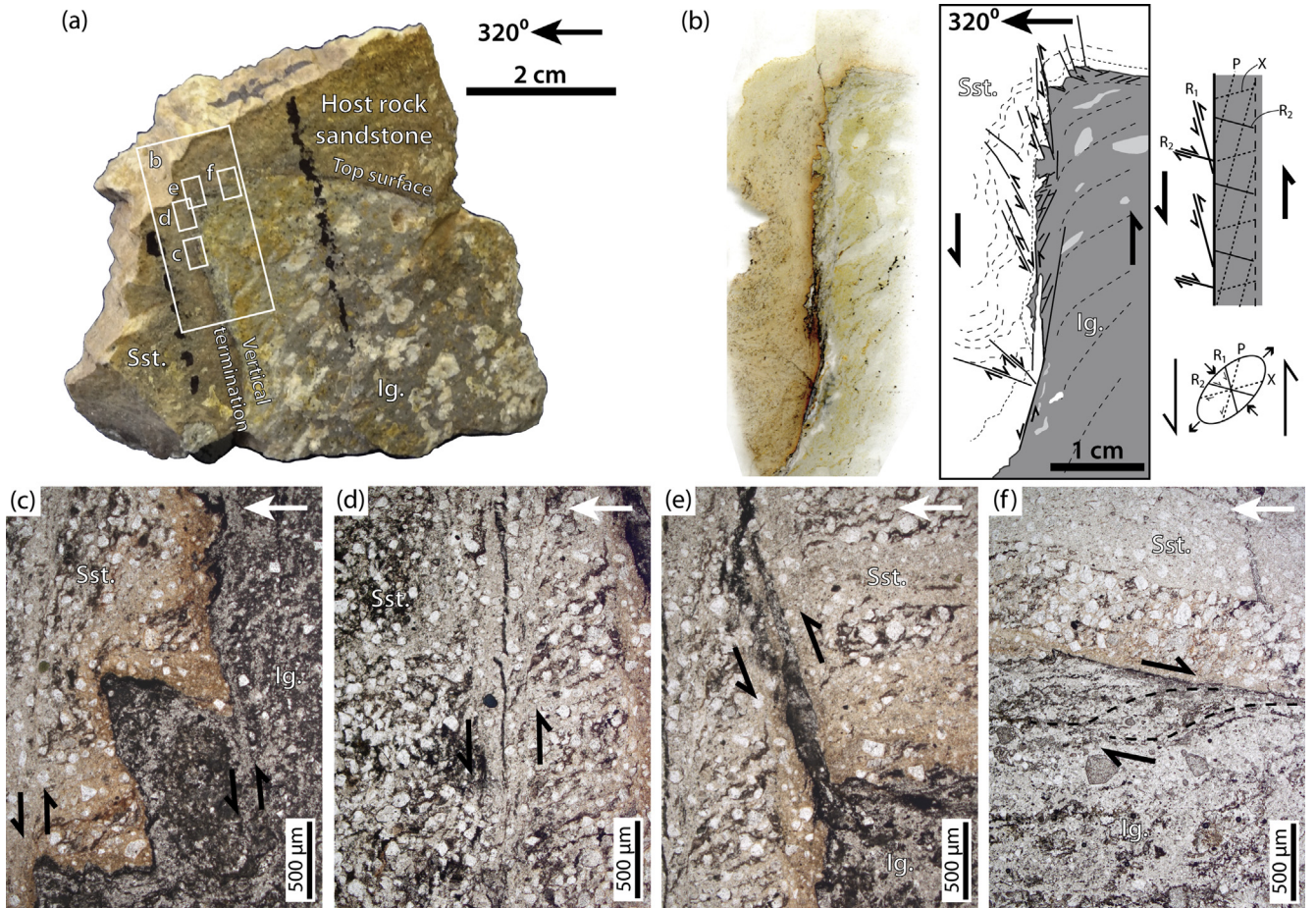


Fig. 13. Photomicrographs of microstructures observed at the intrusion – sandstone contact. (a) Oriented sample highlighting area of thin section and location of images (b)–(f). (b) Thin section and annotated sketch highlighting key structures. (c) Stepped vertical contact at the tip of an intrusive sill sheet. (d) Sub-vertical fracture within host rock adjacent to contact, showing down-to-the-NW movement. (e) Magma injecting upwards along an extensional fracture. (f) Top surface of intrusion showing sharp contact and narrow altered margin.

therefore, likely to be secondary features that modify originally tapered tips. This modification likely occurs during the inflation stage (Fig. 15b). In the “fault controlled” terminations the vertical edge represents a new contact, while “bulbous” terminations are modified top surfaces. The bulbous shape forms if a small amount of lateral expansion also occurs due to the high magma pressure required for vertical growth. The bulbous geometry would be consistent with the tip region containing solidified but still plastic material (e.g. similar to the leading edge of basalt pillows).

Using finite element modelling, Smart et al. (2010) examined the strain distribution in monoclinaly deformed beds overlying a steeply dipping extensional fault, noting the development of outer and inner arc strain domains in the folds (e.g. Frehner, 2011). They also identified a zone of high sub-horizontal extensional strain within the footwall block (see Fig. 11 in Smart et al., 2010). This local extensional strain domain may provide a mechanism for the inflation at the sill tip to form the observed bulbous terminations. However, the formation of extensional faults at the sill tips will tend to impede the development of bulbous terminations, as this extensional strain will instead be accommodated by fault extension. It is therefore significant that sill sheets with a bulbous character show little evidence for fault development (Morgan et al., 2008), while those with faults at their tips do not exhibit bulbous terminations (e.g. Fig. 4d; this study).

6.4.3. Stage 3a – emplacement of additional sill sheets

Successive sheets were emplaced by the same two-stage process (i.e. radial followed by vertical growth) as for the first sill sheet. Along the western transect (TMTW), the sequence of sill sheet stacking was largely from the bottom of the intrusion upwards, as each successive sill sheet was emplaced on top of the underlying sheet, i.e. over-accretion. Along the western transect (TMTW) we see evidence for at least four stacked sill sheets (Fig. 4a). However, on the eastern transect (TMTE), the sequence and level at which successive sheets were emplaced varies significantly with under- and mid-accretion of sheets (see Section 6.5); field observations indicate ~5 parallel sheets intruding beneath two inclined sheets.

6.4.4. Stage 3b – onset of sill-climbing/transgression

Following the formation of P2B faults during the vertical inflation stage, magma was able to utilise these faults and sill-climbing commenced (Fig. 14; Thomson and Schofield, 2008). Dilation of the fault allows magma ingress along the fault plane (Figs. 14 and 15c). At Trachyte Mesa, examples of sill climbing can be observed both at outcrop (Figs. 4c and 5c) and in thin section (Fig. 12e). This process preferentially exploited reverse dip-slip faults (Fig. 15c) for two likely reasons. The first is that the geometry of the reverse faults, dipping towards the sill termination, allowed the magma to continue its outward radial flow up along the fault plane and up through the host stratigraphy. The second factor controlling sill

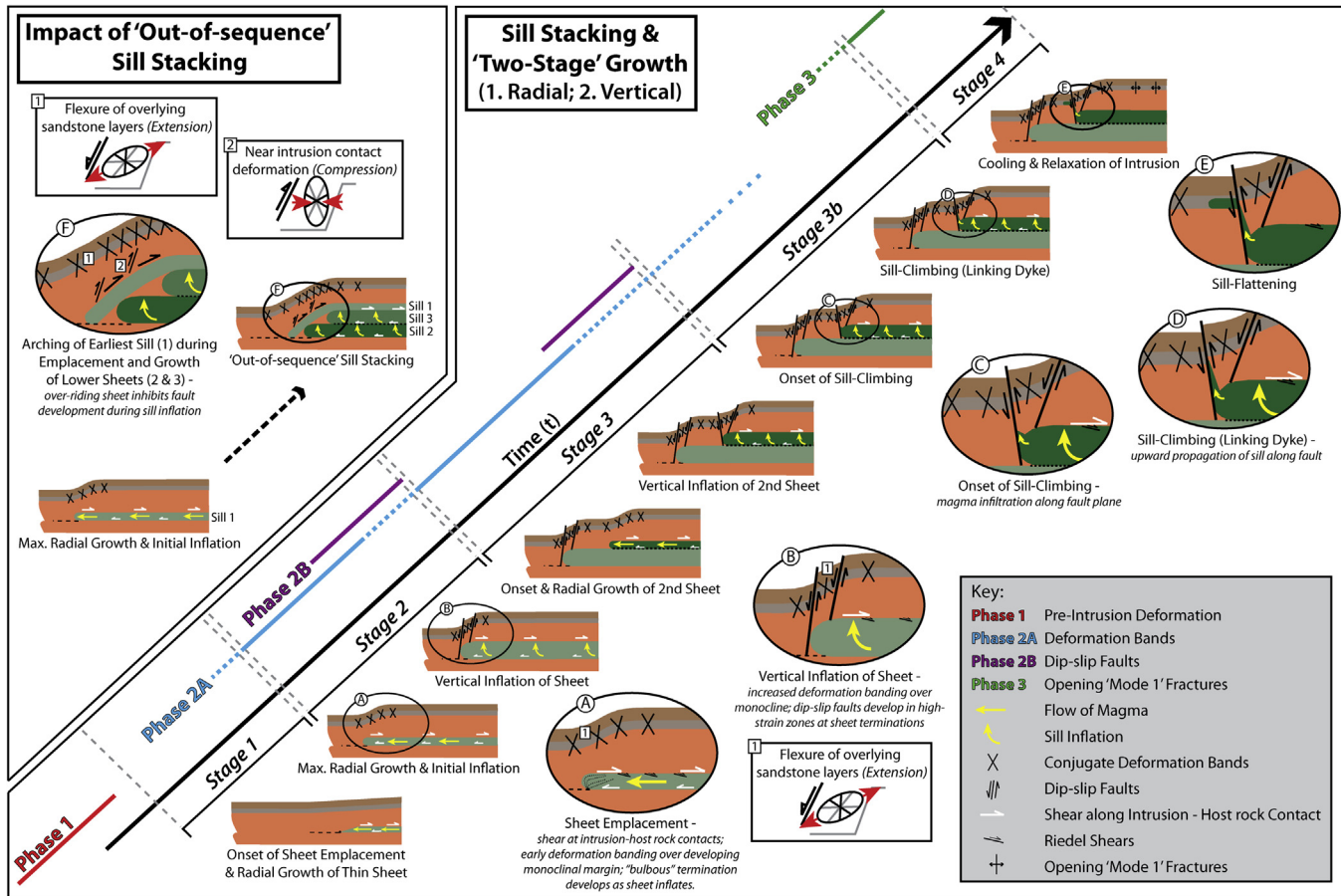


Fig. 14. Schematic diagram outlining a two-stage growth model for sill emplacement at the Trachyte Mesa intrusion and associated deformation structures. Over-accretion stacking model (as observed at TMTW study area; see cross-section in [Supplementary information](#)). Stages of emplacement, as discussed in text, are: Stage 1 – Sill initiation and radial growth as a thin “proto-” sill sheet; Stage 2 – Thickening of the sill sheet, resulting in roof uplift and strain localisation in the host rock at the sill sheet termination; Stage 3 – Emplacement of a second sill sheet (repetition of stages 1 and 2 for 2nd sheet); Stage 3b – Sill climbing through the exploitation of faults developed during Stage 2; Stage 4 – Sill flattening (not observed at Trachyte Mesa) and late stage cooling and relaxation of the intrusion. Schematic illustration (top left) highlighting the impact of out-of-sequence (under- and mid-accretion) stacking [equivalent to Stages 2 and 3 in (a)] on margin geometry and deformation structures (as observed in TMTE study area; see cross-section in [Supplementary information](#)).

climbing along these faults is the stress induced on the fault due to roof uplift (Fig. 15c). If the P2B faults have a normal geometry (i.e. dipping away from the sill sheet), vertical compressive stress associated with uplift of the underlying footwall block (i.e. vertical inflation of sill sheet) will keep the plane closed and prevent migration of magma along its path (Fig. 15c). In contrast, if the fault has a reverse geometry (i.e. dipping towards the sill sheet) uplift of the hangingwall block reduces the vertical normal stress, thus enabling magma to exploit the fault plane (Fig. 15c). Interestingly, such sill climbing processes associated with the exploitation of peripheral faults are likely to play a significant role in the development of the saucer-shaped sills widely imaged in offshore seismic reflection data from sedimentary basins (Thomson and Schofield, 2008; Galland et al., 2009).

6.4.5. Stage 4 – cooling and relaxation of intrusion

As the intrusive sheets (and overall intrusive body) started to cool and contract with the cessation of magma flow, the host rocks above also relaxed. During this relaxation phase, tensile joints developed in response to changes in both flexural and thermal stresses in the vicinity of the intrusion, allowing hydrothermal fluids to circulate (Figs. 7g, h and 14).

6.5. Sequence of stacking

The sequence in which intrusive sill sheets are stacked plays a significant role in the resulting geometry of the intrusion, as well as the types of deformation structures observed in the overlying host rocks. In the two structural transects carried out here (Fig. 3; also see cross-sections in [Supplementary information](#)), contrasting styles of intrusion geometry are observed that are the result of different orders of sill stacking. The lack of continuity of sills sheets between the two transects likely reflects a complex morphology of stacked lobate geometries (see Fig. 4b; see also Fig. 14 in Morgan et al., 2008) with different accretion histories. On the western transect, the margin of the intrusion is characterised by a series (≥ 4) of sub-horizontal sill sheets of varying thickness (0.5–3 m) stacked one on top of the other, i.e. over-accretion (Fig. 14). In contrast, on the eastern transect the order of sill stacking appears out-of-sequence (under- and/or mid-accretion; Menand, 2008). As discussed by Morgan et al. (2008), it appears here that the lower sub-horizontal sheets were emplaced later than upper sheets. The main evidence for this out-of-sequence stacking is the fact that the upper sill sheets have been arched and rotated into a similar monoclinal geometry to the overlying sandstone beds due to the emplacement of sub-horizontal sheets beneath. Not only does the sequence of stacking affect the geometry of the intrusion, it also has

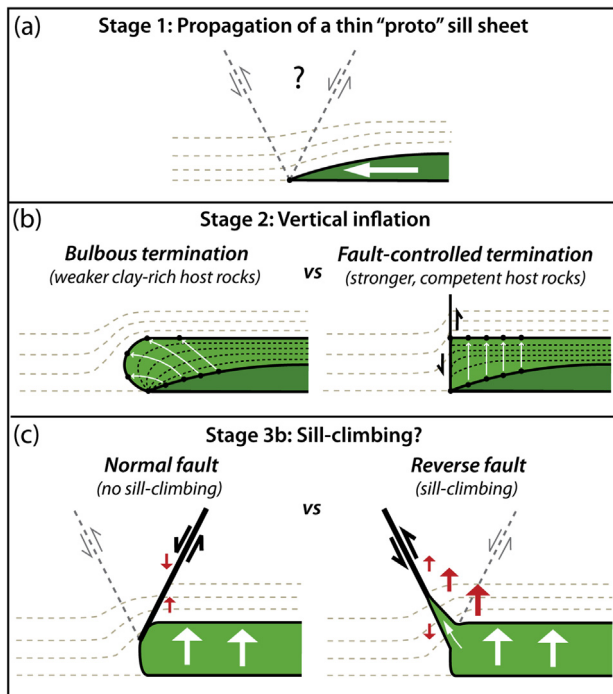


Fig. 15. Transition from horizontal propagation to vertical growth of sill sheets. (a) Lateral propagation of a thin “proto” sill sheet. Note the wedge-shaped tip geometry. Bedding is moderately deformed by flexure and distributed deformation. No fault development, i.e. no strain localisation. (b) Vertical inflation of sill sheets. The development of “bulbous” versus “fault-controlled” terminations is controlled by overlying host-rock lithology and their mechanical properties. (c) Development of dip slip faults at sill tips during two-stage growth model and implications for sill climbing and vertical propagation. Normal faults inhibit magma propagation (due to vertical stress associated with uplift of underlying footwall block). Reverse faults permit sill-climbing (uplift of the hangingwall block reduces the vertical normal stress allowing magma to exploit and propagate along the fault).

a significant impact on the style of deformation occurring in the overlying host rock. In a sequentially stacked sequence (e.g. TMTW) a “stepped” bedding profile is developed (i.e. terraces associated with individual sill sheets), and dip-slip faults (P2B) occur at the tips of successive intrusive sheets. In areas where out-of-sequence emplacement occurs (e.g. TMTE), the intrusion margin is distinctly monoclinal (i.e. one single smooth step) and, due to the presence of the overlying sill sheets, the development of P2B faults is inhibited (Fig. 14). Close to the intrusion contact, compressional deformation structures including small reverse faults are observed, although in the more competent sandstone beds, extension-dominated deformation structures still prevail (Fig. 7b).

7. Conclusions

The Trachyte Mesa intrusion comprises a series of stacked sill sheets. Deformation structures associated with the emplacement of the intrusion are very well preserved and vary in style and intensity along the intrusion margin. Detailed analysis of these host rock deformation structures and their cross-cutting relationships enables the recognition of three distinct phases, interpreted to represent pre- (P1), syn- (P2), and late-stage (P3) emplacement deformation stages. The close spatial and kinematic association of P2 structures indicate extensional strain normal to the intrusion margin during emplacement, with the inclination of the sigma-3 axis reflecting the flexure during vertical inflation episodes along the margin. Strain localisation and extensional faulting at sill sheet terminations, and sill climbing, support a “two-stage growth”

history for both individual sheets and the overall intrusion. These observations are analogous to models of sill emplacement (e.g. Pollard and Johnson, 1973; Thomson and Schofield, 2008).

Deformation structures record the strain evolution, and thus provide a valuable tool to understand the mode of emplacement of the intrusion. The order in which the sill sheets are stacked (i.e. under-, mid-, over-accretion) has a significant impact both on the intrusion geometry and associated deformation. Consequently, the presence or absence of specific deformation structures (e.g. 2B faults) may be key to discriminating the sequence of sill-stacking.

Acknowledgements

The terrestrial laser scanning field work carried out in this paper was funded by the Geological Society’s Elspeth Matthews Award for Fieldwork. Thanks to Midland Valley for providing an academic licence for the use of Move™ and FieldMove™ software in this study. The authors would like to thank S. Cruden and T. Menand for their constructive and positive reviews. C. Magee and S. Morgan provided valuable discussions, comments and feedback on earlier drafts of the manuscript. P.W. would also like to thank to S. Gunnell and S. Nelson for their support and assistance in the field.

Appendix A. Supplementary data

Supplementary data related to this article can be found at <http://dx.doi.org/10.1016/j.jsg.2016.04.001>.

References

- Annen, C., Blundy, J.D., Sparks, R.S.J., 2008. The sources of granitic melt in deep hot zones. *Trans. Roy. Soc. Edinb. Earth Sci.* 97, 297–309.
- Aydin, A., 1978. Small faults formed as deformation bands in sandstone. *Pure Appl. Geophys.* 116, 913–930.
- Bachmann, O., Bergantz, G., 2008. The magma reservoirs that feed supereruptions. *Elements* 4, 17–21.
- Bump, A.P., Davis, G.H., 2003. Late Cretaceous – early Tertiary Laramide deformation of the northern Colorado Plateau, Utah and Colorado. *J. Struct. Geol.* 25, 421–440.
- Bunger, A.P., Cruden, A.R., 2011. Modelling the growth of laccoliths and large mafic sills: role of magma body forces. *J. Geophys. Res.* 116, B02203. <http://dx.doi.org/10.1029/2010JB007648>.
- Corry, C.E., 1988. Laccoliths: mechanics of emplacement and growth. *Geol. Soc. Am. Special Papers*, 110 pp.
- Cosgrove, J.W., Hiller, R.D., 1999. Forced-fold development within Tertiary sediments of the Alba Field, UKCS: evidence of differential compaction and post-depositional sandstone remobilization. In: Cosgrove, J.W., Ameen, M.S. (Eds.), *Forced Folds and Fractures*, vol. 169. Geological Society of London Special Publication, pp. 61–71.
- Cruden, A.R., McCaffrey, K.J.W., 2001. Growth of plutons by floor subsidence: implications for rates of emplacement, intrusion spacing and melt-extraction mechanisms. *Phys. Chem. Earth Part A Solid Earth Geod.* 26, 303–315.
- Cruden, A.R., McCaffrey, K.J.W., 2006. Dimensional scaling relationships of tabular igneous intrusions and their implications for a size, depth and compositionally dependent spectrum of emplacement processes in the crust. *Eos Trans. AGU* 87 (52). Fall Meet. Suppl., Abstract V12B-06.
- Davis, G.H., 1978. Monocline fold pattern of the Colorado Plateau. In: Matthews, V.I. (Ed.), *Laramide Folding Associated with Basement Block Faulting in the Western United States*, vol. 151. Geological Society of America Memoir, pp. 215–233.
- Davis, G.H., 1999. Structural Geology of the Colorado Plateau Region of Southern Utah, with Special Emphasis on Deformation Bands, vol. 342. Geological Society of America, Special Papers.
- De Paola, N., Holdsworth, R.E., McCaffrey, K.J.W., Barchi, M.R., 2005. Partitioned transtension: an alternative to basin inversion models. *J. Struct. Geol.* 27, 607–625.
- de Saint Blanquat, M., Tikoff, B., 1997. Development of magmatic to solid-state fabrics during syntectonic emplacement of the Mono Creek Granite, Sierra Nevada Batholith. In: Bouchez, J.L., Hutton, D.H.W., Stephens, W.E. (Eds.), *Granite: from Segregation of Melt to Emplacement Fabrics*. Kluwer Academic Publishers, Dordrecht, pp. 231–252.
- de Saint Blanquat, M., Habert, G., Horsman, E., Morgan, S., Tikoff, B., Launeau, P., Gleizes, G., 2006. Mechanisms and duration of non-tectonically assisted magma emplacement in the upper crust: Black Mesa pluton, Henry Mountains, Utah. *Tectonophysics* 428, 1–31. <http://dx.doi.org/10.1016/j.tecto.2006.07.014>.
- Du Toit, A.L., 1920. *The Karoo dolerites of South Africa: a study in hypabyssal*

- injection. *Trans. Geol. Soc. S. Afr.* 23, 1–42.
- Engel, C.G., 1959. Igneous rocks and constituent hornblende of the Henry Mountains, Utah. *Geol. Soc. Am. Bull.* 70, 951–980. [http://dx.doi.org/10.1130/0016-7606\(1959\)70\[951:IRACH\]2.0.CO;2](http://dx.doi.org/10.1130/0016-7606(1959)70[951:IRACH]2.0.CO;2).
- Frehner, M., 2011. Neutral lines in buckle folds. *J. Struct. Geol.* 33, 1501–1508.
- Galland, O., Planke, S., Neumann, E.-R., Malthe-Sørensen, A., 2009. Experimental modelling of shallow magma emplacement: application to saucer-shaped intrusions. *Earth Planet. Sci. Lett.* 277, 373–383. <http://dx.doi.org/10.1016/j.epsl.2008.11.003>.
- Gilbert, G.K., 1877. Geology of the Henry Mountains, Utah, 170 pp. U.S. Geological and Geological Survey of the Rocky Mountain Region.
- Gilbert, G.K., 1896. Laccolites in southeastern Colorado. *J. Geol.* 4, 816–825.
- Glazner, A.F., Bartley, J.M., Coleman, D.S., Gray, W., Taylor, R.Z., 2004. Are plutons assembled over millions of years by amalgamation from small magma chambers? *GSA Today* 14. [http://dx.doi.org/10.1130/1052-5173\(2004\)013!0004:APAOMOO](http://dx.doi.org/10.1130/1052-5173(2004)013!0004:APAOMOO).
- Habert, G., de Saint Blanquat, M., 2004. Rate of construction of the Black Mesa bysmalith, Henry Mountains, Utah, USA. In: Breitkreutz, C., Petford, N. (Eds.), *Physical Geology of High-level Magmatic Systems*. Geological Society, London, pp. 143–159. Special Publication 234.
- Hintze, L.E., Kowallis, B.J., 2009. A Field Guide to Utah's Rock: Geological History of Utah. Brigham Young University Geology Studies Special Publication 9, 225 pp.
- Holdsworth, R.E., McErlean, M.A., Strachan, R.A., 1999. The influence of country rock structural architecture during pluton emplacement: the Loch Loyal syenites, Scotland. *J. Geol. Soc. Lond.* 156, 163–175.
- Horsman, E., Tikoff, B., Morgan, S., 2005. Emplacement related fabric in a sill and multiple sheets in the Maiden Creek sill, Henry Mountains, Utah. *J. Struct. Geol.* 27, 1426–1444. <http://dx.doi.org/10.1016/j.jsg.2005.03.003>.
- Hunt, C.B., 1953. Geology and Geography of the Henry Mountains Region, Utah. U.S. Geological Survey Professional Paper 228, 234 pp.
- Hunt, C.B., 1988. Geology of the Henry Mountains, Utah, as recorded in the notebooks of G.K. Gilbert, 1975–1876. *Geol. Soc. Am. Mem.* 167, 229 pp.
- Hutton, D.H.W., Dempster, T.J., Brown, P.E., Decker, S.D., 1990. A new mechanism of granite emplacement: intrusion in active extensional shear zones. *Nature* 343, 452–455.
- Jackson, S.E., Pollard, D.D., 1988. The laccolith-stock controversy: new results from the southern Henry Mountains, Utah. *Geol. Soc. Am. Bull.* 100, 117–139. <http://dx.doi.org/10.1130/0016-7606>.
- Johnson, A.M., Pollard, D.D., 1973. Mechanics of growth of some laccolithic intrusion in the Henry Mountains, Utah, I: field observations, Gilbert's model, physical properties and flow of the magma. *Tectonophysics* 18, 261–309. [http://dx.doi.org/10.1016/0040-1951\(73\)90050-4](http://dx.doi.org/10.1016/0040-1951(73)90050-4).
- Johnson, K.M., Johnson, A.M., 2002. Mechanical analysis of the geometry of forced-folds. *J. Struct. Geol.* 24, 401–410.
- Jones, R.R., McCaffrey, K.J.W., Clegg, P., Wilson, R.W., Holliman, N.S., Holdsworth, R.E., Imber, J., Waggett, S., 2009. Integration of regional to outcrop digital data: 3D visualisation of multi-scale geological models. *Comput. Geosci.* 35, 4–18.
- Jowett, E.C., Robin, P.-Y.F., 1988. Statistical significance of clustered orientation data on the sphere: an empirical derivation. *J. Geol.* 96, 591–599.
- Larson, M.J., Bromfield, C.S., Dubiel, R.F., Patterson, C.G., Peterson, F., 1985. Geologic Map of the Little Rockies Wilderness Study Area and the Mt. Hillers and Mt. Pennell Study Areas, and Vicinity, Garfield County, Utah. U.S. Geological Survey Map MF-1776-B.
- Magee, C., Stevenson, C.T., O'Driscoll, B., Petronis, M., 2012. Local and regional controls on the lateral emplacement of the Ben Hiant dolerite intrusion, Ardnamurchan (NW Scotland). *J. Struct. Geol.* 39, 66–82. <http://dx.doi.org/10.1016/j.jsg.2012.03.005>.
- Magee, C., Jackson, C.A.-L., Schofield, N., 2014. Diachronous sub-volcanic intrusion along deep-water margins: insights from the Irish Rockall Basin. *Basin Res.* 26, 85–105. <http://dx.doi.org/10.1111/bre.12044>.
- Mahan, K.H., Bartley, J.M., Coleman, D.S., Glazner, A.F., Carl, B., 2003. Sheeted intrusion of the synkinematic McDoole pluton, Sierra Nevada, California. *Geol. Soc. Am. Bull.* 115, 1570–1582.
- Marshak, S., Paulsen, T., 1996. Midcontinent U.S. fault and fold zones: a legacy of Proterozoic intracratonic extensional tectonism? *Geology* 24, 151–154.
- McCaffrey, K.J.W., 1992. Igneous emplacement in a transpressive shear zone: Ox Mountains igneous complex. *J. Geol. Soc. Lond.* 149, 221–235.
- McCaffrey, K.J.W., Jones, R.R., Holdsworth, R.E., Wilson, R.W., Clegg, P., Imber, J., Holliman, N., Trinks, I., 2005. Unlocking the spatial dimension: digital technologies and the future of geoscience fieldwork. *J. Geol. Soc. Lond.* 162, 927–938.
- Menand, T., 2008. The mechanics and dynamics of sills in layered elastic rocks and their implications for growth of laccoliths and other igneous complexes. *Earth Planet. Sci. Lett.* 267, 93–99. <http://dx.doi.org/10.1016/j.epsl.2007.11.043>.
- Menand, T., de Saint Blanquat, M., Annen, C.J., 2011. Emplacement of magma pulses and growth of magma bodies. *Tectonophysics* 500, 1–2. <http://dx.doi.org/10.1016/j.tecto.2010.05.014>.
- Morgan, S., Horsman, E., Tikoff, B., de Saint Blanquat, M., Nugent, A., Habert, G., 2005. Sheet-like emplacement of satellite laccoliths, sills and bysmaliths of the Henry Mountains, southern Utah. In: Pederson, J., Dehler, C.M. (Eds.), *Interior Western United States Field Guide*, vol. 6. GSA Field Guide, pp. 283–309. [http://dx.doi.org/10.1130/2005.fld006\(14\)](http://dx.doi.org/10.1130/2005.fld006(14)).
- Morgan, S., Stanik, A., Horsman, E., Tikoff, B., de Saint Blanquat, M., Habert, G., 2008. Emplacement of multiple magma sheets and wall rock deformation: Trachyte Mesa intrusion, Henry Mountains, Utah. *J. Struct. Geol.* 30, 491–512. <http://dx.doi.org/10.1016/j.jsg.2008.01.005>.
- Nelson, S.T., Davidson, J.P., Sullivan, K.R., 1992. New age determinations of central Colorado Plateau laccoliths, Utah: recognizing disturbed K–Ar systematics and re-evaluating tectonomagmatic relationships. *Geol. Soc. Am. Bull.* 104, 1547–1560.
- Nelson, S.T., Davidson, J.P., 1993. Interactions between mantle-derived magmas and mafic crust, Henry Mountains, Utah. *J. Geophys. Res.* B2 98, 1837–1852.
- Neves, S.P., Vauchez, A., Archanjo, C.J., 1996. Shear zone-controlled magma emplacement or magma-assisted nucleation of shear zones? Insights from northeast Brazil. *Tectonophysics* 262, 349–364.
- Passchier, C.W., Zhang, J.S., Konopasek, J., 2005. Geometric aspects of synkinematic granite intrusion into a ductile shear zone — an example from the Yunmengshan core complex, northern China. In: Bruhn, D., Burlini, L. (Eds.), *High-strain Zones: Structure and Physical Properties*, 245. Geological Society London, pp. 65–80. <http://dx.doi.org/10.1144/GSL.SP.2005.245.01.04>. Special Publication.
- Pitcher, W.S., 1970. Ghost stratigraphy in intrusive granites: a review. In: Newall, G., Rast, N. (Eds.), *Mechanism of Igneous Intrusion*. Gallery Press, Liverpool, pp. 123–140.
- Pollard, D.D., Johnson, A.M., 1973. Mechanics of growth of some laccolithic intrusions in the Henry Mountains, Utah, II: bending and failure of overburden layers and sill formation. *Tectonophysics* 18, 261–309.
- Pollard, D.D., Muller, O.H., Dockstader, D.R., 1975. The form and growth of fingered sheet intrusions. *Geol. Soc. Am. Bull.* 3, 351–363.
- Price, N.J., 1966. *Faults and Joint Development in Brittle and Semi-brittle Rock*. New York Pergamon Press.
- Reches, Z., 1987. Determination of the tectonic stress tensor from slip along faults that obey the Coulomb yield condition. *Tectonics* 6, 849–861.
- Schofield, N.J., Brown, D.J., Magee, C., Stevenson, C.T., 2012. Sill morphology and comparison of brittle and non-brittle emplacement mechanisms. *J. Geol. Soc. Lond.* 169, 127–141.
- Seers, T.D., Hodgetts, D., 2013. Comparison of digital outcrop and conventional data collection approaches for the characterization of naturally fractured reservoir analogues. In: Spence, G.H., Redfern, J., Aguilera, R., Bevan, T.G., Cosgrove, J.W., Couples, G.D., Daniel, J.M. (Eds.), *Advances in the Study of Fractured Reservoirs*, vol. 374. Geological Society of London, pp. 51–77. <http://dx.doi.org/10.1144/SP374.13>. Special Publication.
- Smart, K.J., Ferrill, D.A., Morris, A.P., Bichon, B.J., Riha, D.S., Huyse, L., 2010. Geomechanical modeling of an extensional fault-propagation fold: Big Brushy Canyon monocline, Sierra Del Carmen, Texas. *AAPG Bull.* 94, 221–240. <http://dx.doi.org/10.1306/08050908169>.
- Schmidt, W., 1925. Gefügestatistik Tschermark Mineral. *Petrogr. Mitt* 38, 392–423.
- Stearns, D.W., 1978. Faulting and forced folding in the Rocky Mountains foreland. *Geol. Soc. Am. Mem.* 151, 1–37.
- Stevenson, C.T.E., Owens, W.H., Hutton, D.H.W., Hood, D.N., Meighan, I., 2007a. Laccolithic, as opposed to cauldron subsidence, emplacement of the Eastern Mourne pluton: evidence from anisotropy of magnetic susceptibility. *J. Geol. Soc. Lond.* 164, 99–110. <http://dx.doi.org/10.1144/0016076492006-008>.
- Stevenson, C.T.E., Owens, W.H., Hutton, D.H.W., 2007b. Flow lobes in granite: the determination of magma flow direction in the Trawenagh Bay Granite, north-western Ireland, using anisotropy of magnetic susceptibility. *GSA Bull.* 119, 1368–1386. <http://dx.doi.org/10.1130/B25970.1>.
- Thomson, K., 2004. Sill complex geometry and internal architecture: a 3D seismic perspective. In: Breitkreutz, C., Petford, N. (Eds.), *Physical Geology of High-level Magmatic Systems*, vol. 234. Geological Society London, pp. 229–232. Special Publication.
- Thomson, K., 2004. Geometry and growth of sill complexes: insights using 3-d seismic from the North Rockall Trough. *Bull. Volcanol.* 66, 364–375.
- Thomson, K., Schofield, N., 2008. Lithological and structural controls on the emplacement and morphology of sills in sedimentary basins. In: Thomson, K., Petford, N. (Eds.), *Structure and Emplacement of High-level Magmatic Systems*, vol. 302. Geological Society London, pp. 31–44. Special Publication.
- Wetmore, P.H., Connor, C.B., Kruse, S.E., Callihan, S., Pignotta, G., Stremtan, C., Burke, A., 2009. Geometry of the Trachyte Mesa intrusion, Henry Mountains, Utah: implications for the emplacement of small melt volumes into the upper crust. *Geochem. Geophys. Geosyst.* 10, Q08006. <http://dx.doi.org/10.1029/2009GC002469>.
- Wilson, P.I.R., McCaffrey, K.J.W., 2013. Intrusion space problem: digital mapping and analysis of the Maiden Creek satellite intrusion, Henry Mountains Utah. *Geoscientist* 23 (6), 16–19.
- Wilson, P.I.R., 2015. Direct Linking of Host Rock Deformation Structures to the Emplacement, Morphology and Accommodation of High-level Igneous Intrusions: the Henry Mountains, Utah (PhD thesis). Kingston University London.
- Withjack, M.O., Olson, J., Peterson, E., 1990. Experimental models of extensional forced folds. *AAPG Bull.* 74, 1038–1054.